TRANSITION STUDIES AND SKIN FRICTION MEASUREMENTS ON AN INSULATED FLAT PLATE AT A HYPERSONIC MACH NUMBER

Thesis by

Robert H. Korkegi

In Partial Fulfillment of the Requirements

For the Degree of

Doctor of Philosophy

California Institute of Technology

Pasadena, California

1954

ACKNOWLEDGMENTS

The writer wishes to thank his advisor, Dr. H. T. Nagamatsu, for his help and encouragement throughout this work. He is greatly indebted to Professors H. W. Liepmann and Lester Lees, and Dr. D. E. Coles for many stimulating discussions and suggestions which influenced appreciably the course of this research, and, especially, to Professor Lees for his critical review of the manuscript.

The help of many members of the Hypersonic staff in instrumentation problems and in carrying out the tests is greatly appreciated. In particular, Mr. R. L. Richmond's assistance in the design of much of the experimental equipment was invaluable.

The writer owes much to Mr. W. M. Sublette of the Aeronautics Machine Shop for his most skillful work in making the intricate precision instruments for the skin friction measurements, and wishes to thank Mr. C. A. Bartsch for his help in problems of fabrication.

Many thanks also go to Miss Fae Scheinis and Mrs. H. Van Gieson for their very able work in the preparation of the plots and the manuscript.

ABSTRACT

An investigation of transition and skin friction on an insulated flat plate, 5 x 26 inches, was made in the GALCIT 5 x 5 inch Hypersonic Wind Tunnel, Leg No. 1, at a nominal Mach number of 5.8.

The phosphorescent lacquer technique was used for transition detection and was found to be in good agreement with total-head rake measurements along the plate surface and pitot boundary layer surveys. It was found that the boundary layer was laminar at Reynolds numbers of at least 5×10^6. It was also observed that transverse contamination due to the turbulent boundary layer on the tunnel sidewall originated far downstream of the flat plate leading edge at Reynolds numbers of 1.5 to 2×10^6, and spread at a uniform angle of $5\frac{1}{2}^\circ$ compared with $9\frac{1}{2}^\circ$ in low speed flow.

The effect of two-dimensional and local disturbances was investigated. The technique of air injection into the boundary layer as a means of stimulating transition was extensively used. It was observed that, although the onset of transition occurred at Reynolds numbers down to 10^6, a fully developed turbulent boundary layer was not obtained at Reynolds numbers much below 2×10^6 regardless of the amount of air injected.

A qualitative discussion of these results is given with emphasis on the possibility of a greater stability of the laminar boundary layer in hypersonic flow than at lower speeds.

Direct skin friction measurements were made by means of the floating element technique incorporating a null system using chain

loading, over a range of Reynolds numbers (based on distance from leading edge) from 10^6 to 4×10^6. Without artificial tripping, the boundary layer was verified as being laminar over the complete range. With air injection, turbulent shear was obtained only for Reynolds numbers greater than 2×10^6, this value being in good agreement with earlier results of this investigation. The turbulent skin friction coefficient was found to be approximately 0.40 of that for incompressible flow for a constant value of R_θ, and 0.46 for an effective Reynolds number between 5 and 6×10^6.

TABLE OF CONTENTS

TABLE OF FIGURES

SYMBOLS

C_f	local skin friction coefficient, τ_w/q
C_F	mean skin friction coefficient
C_p	specific heat at constant pressure (Btu/lb/^oF)
H	boundary layer shape parameter, δ^*/θ
k	thermal conductivity (Btu/sq ft/^oF/hr)
M	Mach number
M_a	mass flow of air jets per unit span (slugs/sec/in)
M_{δ^*}	boundary layer mass defect per unit span, $\rho_\infty u_\infty \delta^*$ (slugs/sec/in)
m	100 x M_a/M_{δ^*} (%)
p	pressure (lbs/sq in)
p_o'	impact or pitot pressure (lbs/sq in)
Pr	Prandtl number, $C_p \mu/k$
q	dynamic pressure, $\frac{1}{2}\rho_\infty u_\infty^2$ (lbs/sq in)
Re	free stream Reynolds number, $u_\infty x/\nu_\infty$
Re/in	Reynolds number per inch, u_∞/ν_∞ (/in)
R_{δ^*}	Reynolds number based on displacement thickness, $u_\infty \delta^*/\nu_\infty$
R_θ	Reynolds number based on momentum thickness, $u_\infty \theta/\nu_\infty$
T	temperature (^oF or ^oR)
u	x-component of velocity (ft/sec)
x	streamwise distance from flat plate leading edge (in)
y	vertical distance from plate surface (in)
γ	ratio of specific heats
δ	boundary layer thickness (based on $u/u_\infty = 0.995$) (in)
δ^*	boundary layer displacement thickness (in)

θ boundary layer momentum thickness (in)

μ absolute viscosity (lb sec/sq ft)

ν kinematic viscosity (sq ft/sec)

ρ density (slugs/cu ft)

τ shear stress (lbs/sq in)

Subscripts

i incompressible value

o stagnation or reservoir conditions

w conditions at wall (flat plate surface)

∞ free stream conditions

Other symbols locally used are defined in the text.

I. INTRODUCTION

Transition and skin friction in the hypersonic regime are presently of great interest. Drag, performance, and heat transfer rates depend on the location of transition on the surface of a body in flight.

While the effects of free stream turbulence, pressure gradients, surface curvature, surface roughness, and heat transfer on transition are at least known qualitatively (Cf. Ref. 1), the effect of compressibility in the high Mach number range is still subject to speculation. At low supersonic Mach numbers various wind tunnel tests indicate a general decrease of transition Reynolds number with increasing Mach number (Cf. Refs. 2 and 3).

What causes transition from laminar to turbulent boundary layers to occur? Tollmien and Schlichting predicted that transition is caused by the selective amplification of small disturbances originating within the laminar boundary layer, and give a limiting Reynolds number (Re_{crit}) below which no amplification can occur. Later, Taylor proposed that turbulence in the free stream produces pressure pulses which cause intermittent separation of the boundary layer and eventual transition. Subsequently, the latter was found to correspond to the case where large free stream turbulence is present, while the former type of instability, verified experimentally by Schubauer and Skramstad (Ref. 4), was found to exist in flows with a very low turbulence level (Cf. Refs. 1 and 5).

Lees and Lin (Refs. 6 and 7) contributed a revision and extension of the small disturbance theory to compressible flows. Van Driest (Ref. 8) made calculations based on the Lees-Lin theory and extended it to the hypersonic regime. His results indicate a substantial decrease in

critical Reynolds number with increasing Mach number for a laminar boundary layer on an insulated flat plate. For example, at a Mach number of 5, the critical Reynolds number is less than 200 compared to a value of about 80,000 in low speed flow. On this basis, one might conclude that compressibility has the effect of decreasing the stability of the boundary layer. It should be noted, however, that transition is also dependent upon the amplification rates and wave lengths of laminar disturbances for which there are presently no calculations for the hypersonic regime.

The present transition studies were prompted by preliminary surveys on a flat plate at a Mach number of 5.8, which indicated extensive laminar layers and the inability of induced disturbances to produce transition at low Reynolds numbers.

The second part of the present research deals with direct measurements of surface shear. Quantitatively, emphasis was placed on turbulent skin friction measurements at a Mach number of 5.8. Theoretically, the state of the art is well exemplified by the large scatter of predictions of turbulent skin friction on an insulated flat plate at high Mach numbers (Cf. Fig. 1, Ref. 9). In the hypersonic regime it is probable that fluctuations of the state properties of air become as important as velocity fluctuations in a turbulent boundary layer. Li and Nagamatsu (Ref. 10) investigated the effect of density fluctuations, and predict a rise in turbulent skin friction coefficient with increasing Mach number at hypersonic speeds due to this effect. An extensive discussion of the theoretical literature on turbulent boundary layers is given by Coles (Ref. 11).

Experimentally, direct measurements of turbulent skin friction on insulated flat plates were made by Dhawan (Ref. 12) in subsonic flow, by Hakkinen (Ref. 13) in the transonic regime, and by Coles (Ref. 11) in supersonic flow. Measurements on bodies of revolution in supersonic flow were made by Chapman and Kester (Ref. 9), and by Bradfield, DeCoursin, and Blumer (Ref. 14). The measurements of Coles which extend the range of knowledge of turbulent surface shear to a Mach number of 4.5 are particularly significant.

The technique employed by the aforementioned investigators and the present writer makes use of a floating element which constitutes a portion of the working surface of a model. The shear force on the element is measured by a sensitive balance system. Developmental work of this technique applied to local measurements of aerodynamic friction was undertaken by Dhawan (Ref. 12) under Liepmann. The present balance system is essentially a modification of Dhawan's with the addition of a null-return device.

II. EXPERIMENTAL EQUIPMENT, INSTRUMENTATION, AND TECHNIQUES

The present research was conducted in the GALCIT 5" x 5" Hypersonic Wind Tunnel, Leg No. 1, at a nominal Mach number of 5.8. All tests were made at a fixed reservoir temperature of 225°F, over a range of reservoir pressures from 35 to 110 psia. The temperature was selected to yield the maximum Reynolds number per inch at the highest pressure, while insuring the absence of condensation of air components in the test section. The upper limit of the pressure range was fixed by the compressor plant mass flow capacity.

A. Experimental Facilities

The wind tunnel is of the closed-return type, permitting continuous operation for periods in excess of eight hours. The required compression for operation at Mach 5.8 is supplied by five stages made up of thirteen Fuller rotary compressors. Purification of the air is effected by its passage through a silica gel dryer for moisture removal*, and a system of carbon and fiberglass filters for removal of oil and other impurities. The presence of oil in the air is due to the lubricating system required by the rotary compressors, and although most of it is filtered out, traces of oil find their way into the test section. Although this factor increased the difficulty of some experiments, it is felt that the reliability of the present data was unaffected. Oil streaks on the model surface spread in the flow direction and were

---

* The very large static temperature drop from the tunnel reservoir to the test section at high Mach numbers necessitates extensive moisture removal from the supply air in order to avoid condensation of water vapor.

very thin compared with the boundary layer thickness. For the skin friction measurements particular care was taken to prevent oil from entering the gap surrounding the floating elements. The high stagnation temperature required at Mach numbers above 4.7 for condensation-free* flow (Cf. Ref. 15) is supplied by a steam heat exchanger. A schematic diagram of the wind tunnel installation showing both Leg No. 1 (Mach 2 to 7) and Leg No. 2 (Mach 4 to 11) is given in Fig. 1.

Steady flow conditions are achieved by automatic control of the reservoir temperature ($\pm\frac{1}{2}^{o}$F) and pressure (sensitivity 1/10 of an inch water pressure). Static pressures on models and along the upper nozzle block centerline are indicated on two silicone multi-manometers with a range of $1\frac{1}{4}$ psi. Total pressure measurements as for boundary layer surveys are taken on a single tube mercury micro-manometer. Model temperatures are indicated on a Brown potentiometer. Flow visualization is effected through a schlieren system with mirrors mounted on rails permitting axial traverse of the tunnel test section. Fig. 2 shows a section of the control room with, from left to right, part of the compressor plant motor and valve controls, the two multi-manometers, and the temperature recorder and controller. A more extensive description of the experimental facilities is presented in Ref. 16.

Certain modifications of the Leg No. 1 test section (Cf. Fig. 3) were made with a view toward greater accessibility to models and associated equipment. In particular, a new integral lower diffuser and

---

* Reference is here made to condensation of oxygen and nitrogen in the air at the very low static temperatures in the test section when the supply air is at room temperature.

center block was designed, provided with a cut-out at the test section for a set of removable insert blocks. Thus, models can be completely assembled on one of the insert blocks and easily mounted in the test section when ready for testing (Cf. Fig. 9).

B. Transition and Boundary Layer Surveys

1. The Flat Plate -- Choice of Size and Location

The extensive laminar layers noted on flat plates at Mach 5.8 in the present tunnel pointed to the need for a very long model, i.e., high Reynolds numbers, for transition studies. For this purpose, full advantage was taken of the large uniform flow rhombus at this high Mach number, permitting model lengths of the order of 30 in.. A practical limitation was imposed by waves emanating from the tunnel side walls near the nozzle throat and crossing the test section center-line approximately 13 in. downstream, where their strength resulted in a local 5 to 10 per cent rise in free stream static pressure. An allowance for these waves would have demanded a reduction of the plate length beyond any usefulness for transition studies and subsequent turbulent skin friction measurements, while the effect of their presence on the boundary layer on a long flat plate admittedly limited the quantitative interpretation of data in laminar regions. However, as is later shown, extensive laminar layers were observed to exist up to Reynolds numbers of 5×10^6 in spite of these waves.

In the final analysis, it was decided to make the flat plate 26 in. long (Re_{max} of the order of 6×10^6), and to locate the leading edge 6 in. downstream of the throat section (Cf. Fig. 4). The remaining dimensions are a 5 in. span, and a depth of approximately 4/10 in.,

which, with a 3/32 in. bottom cover plate, gives an overall thickness of ½ in. The purpose of the cover plate is to shield pressure tubes and thermocouple leads embedded in grooves along the bottom surface of the plate. Both plate and cover are made of stainless steel for corrosion resistance.

The leading edge angle on the bottom side of the plate is initially 7°, and increases to 25° beyond the first 3/4 in.. The sharp initial angle was chosen to minimize the local strength of the leading edge wave in an attempt to approach idealized conditions. The plate working surface was ground and lapped to a smooth finish.

The flat plate is equipped with 22 orifices for surface pressure measurements, 16 of which are evenly distributed along the centerline, with 6 copper-constantan thermocouples for surface temperatures, and with a spanwise row of small holes 1½ in. behind the leading edge, for air injection into the boundary layer. The location and detail of pressure orifices and thermocouples are given in Fig. 5. The air jet holes have a 0.013 in. diameter and a spacing of 3/16 in. and lead to a common manifold fed by a line extending outside the tunnel to a flow-meter. Atmospheric air was used for the jets, and the flow rate was controlled by a needle valve and registered on the flow-meter.

The flat plate is supported in the test section by a windshield extending from the center of the plate to the trailing edge, through which pressure tubes and thermocouple leads are guided outside the tunnel, and a vertical strut of adjustable length 6 in. behind the leading edge for levelling purposes.

2. Survey Instruments

The impact pressure probe used for boundary layer surveys on the flat plate consists of 0.042 in. O.D. - 0.022 in. I.D. stainless steel tubing squeezed at the mouth to a 0.004 x 0.030 in. opening with a 0.006 in. wall thickness. The downstream tube size is progressively increased in order to reduce response time. The probe is supported in the test section by a two-strut vertical actuator system which controls the probe position to within 0.001 in. (Cf. Fig. 6).

Boundary layer surveys on the sidewall of the test section were made with an L-shaped impact pressure tube mounted in a small hole in the wall and bent upstream.

Two techniques were used for transition detection: (1) a luminescent lacquer discussed in the following section; and (2) a traversing total-head rake. The total-head rake consists of seven tubes of 0.042 in. O.D. evenly spaced across half the 5 in. span and 1/16 in. above the surface of the flat plate (Cf. Fig. 7). The vertical attitude of the tubes was chosen to yield a substantial increment in impact pressure between laminar and turbulent boundary layers which, over a large extent of the plate, were of the order of 1/5 to 1/2 in. thick. The tubes are supported by a transverse bar with a sharp leading edge and then routed through a 1/4 in. shaft 30 in. long, which extended downstream into the tunnel diffuser section. The transverse bar is equipped with small rollers to guide it between the tunnel sidewalls and over the plate surface. Axial traverse was effected by a manually-operated rack and pinion drive mechanism.

3. Luminescent Lacquer Technique

This technique for transition detection is dependent upon the more rapid drying of a lacquer compound in turbulent areas than in laminar ones. Phosphor pigment in the lacquer gives it the property of fluorescing under ultra-violet irradiation when dry while remaining dark when wet, thus visually defining regions of turbulence. Such a lacquer was developed and successfully used by Stalder and Slack (Ref. 17) at the Ames Aeronautical Laboratory; however, it was not suitable at the high reservoir temperatures (and, consequently, high model surface temperatures) required at hypersonic speeds. Development of the lacquer used in the present research was undertaken at GALCIT by the Hypersonic staff (Ref. 16). Its composition by volume is as follows:

50% Phosphor Pigment*

50% Solvent:

- 10% Ethanol
- 10% Butanol
- 10% Ethyl Cellosolve
- 50% Butyl Carbitol
- 20% Plasticizer (dibutyl phthalate or dibutyl sebacate)

Drying time under the present operating conditions -- T_o 225°F, P_o from 35 to 95 psia -- is as follows:

Plasticizer	Drying Time (Minutes)	
	Turbulent	Laminar
Dibutyl Phthalate	2-10	
Dibutyl Sebacate	10-20	30-

The lacquer was finely sprayed on the surface of the flat plate with an air gun.

---

* T-400 dye mixture, Vogel Luminescense Corp., San Francisco, Calif.

C. Skin Friction Balance

1. Flat Plate

A flat plate identical in geometry and similar in construction to that used for transition studies was fitted with two floating elements for local surface shear measurements. The elements are located on the plate centerline 15½ in. and 23 in., respectively, from the leading edge.* The plate has a row of holes for air injection and five orifices for surface pressure measurements in common with the transition survey plate. In view of the identical location of both plates in the test section and the good repeatability of flow conditions in the tunnel, pressure distributions were taken with the survey plate, while the five orifices served as check points. Agreement was found to be within ±2%. It should be noted, however, that the static pressures used for reduction of the shear data were measured in the chamber housing the skin friction balance, and not on the survey plate.

A partially-hollowed windshield ½ in. wide, mounted on an insert block in the test section, serves the dual purpose of supporting the plate in the tunnel and housing the skin friction balance systems. The plate mounted in the tunnel and part of the equipment associated with the force measurements are shown in Fig. 8. Fig. 9 illustrates the plate and balance completely assembled on a test section insert block (Cf. Experimental Facilities), mounted on a working stand.

---

* Since the primary objective was the measurement of turbulent skin friction, the extensive downstream location of the elements was necessitated by the inability of artificial disturbances to induce transition at low Reynolds numbers.

2. General Balance Design Requirements

In view of the extensive development of instruments, by previous investigators (Cf. Introduction), for the direct measurement of skin friction, only aspects of particular interest in the present design are discussed here. These are the following:

(1) sensitivity of the instrument

(2) effect of tunnel vibrations

(3) thermal effects

(4) gap effects

The sensitivity of the skin friction instrument is determined by the error in force measurements induced by practical limitations of the system. Sensitivity is thus dependent upon the repeatibility of the instrument, the accuracy with which displacement of the floating element can be measured, and any scatter induced by a null-return device, if one is used.

The instrument is subject to wind tunnel vibrations. Hence, it is desirable to design the instrument so that its frequency spectrum is substantially different from that of the tunnel. Ideally, a single degree of freedom system with a very low natural frequency compared to the tunnel frequencies would tend to minimize the effect of the latter. This condition can be approximated in practice by making the floating element and the associated structure extremely compact such as to approach a mass of infinite rigidity, while the suspension (flexures) or pivot assembly can be designed to yield a favorable natural frequency.

Thermal effects are usually severe, especially at hypersonic speeds for which high stagnation temperatures are required. Differential

expansion of the component parts of the balance may produce null shifts (changes in zero reading), changes in calibration, distortion, and misalignment of the floating element with respect to the flat plate surface.

Symmetry of the instrument and position-sensing equipment with respect to the plane of the floating element will minimize shifts in null position. In addition, the shift can be accounted for by taking a null reading under operating conditions after thermal equilibrium has been established. This can be accomplished by shielding the floating element from the air stream.

Changes in calibration, distortion, and misalignment cannot be tolerated to any appreciable degree; hence, compensation for these has to be incorporated in the design. A force-displacement calibration of a flexure linkage instrument is dependent upon the elastic properties of the flexures. Variation of these properties is negligible at moderate temperatures but becomes important at high temperatures. This does not obviate the possibility of using a flexure linkage instrument at hypersonic speeds but illustrates the necessity of using a null-return system. In this type of system, the element is always returned to its null position by the application of some restoring force, thus removing calibration dependence on the flexure properties. It should be noted, however, that the null-return mechanism must, of necessity, be insensitive to temperature. Element misalignment and distortion can be minimized in three ways: by consistent use of materials with almost identical thermal properties for both instrument components and flexures; by use of low expansion alloys such as Invar (36% nickel alloy steel); and by making the instrument compact so as to minimize total differential expansion.

The gap around the floating element produces a surface discontinuity which results in an increase in measured shear. When the gap width is small compared to the boundary layer thickness, one may conservatively estimate a drag increase proportional to the area of the gap (Cf. disucssion in Refs. 11 and 13). For example, were the gap area 3% of that of the element (as is the case for the present instrument), the induced error in surface shear would be at most 3%. This illustrates the advantage of a null-return system in that it imposes no restrictions on the gap size, allowing it to be as small as practically possible.

3. Floating Element Unit

The basic design of the instrument is essentially that of Dhawan (Ref. 12), with particular emphasis placed on compactness and temperature insensitivity. The floating element is fixed to a vertical frame suspended by two thin flexures to a 1-3/4 in. diameter circular disk, which is provided with a rectangular slot for the element. The disk, when inserted into a cut-out in the flat plate, constitutes part of the working surface. The unit is thus self-contained and can be easily removed from the flat plate without requiring disassembly of its component parts. An exploded view shown in Fig. 11 will assist the following discussion.

The floating element has a 1 in. by $\frac{1}{4}$ in. surface separated from the sides of the slot in the circular disk by a 0.003 in. clearance gap. Below a depth of 0.005 in., the sides of the element are beveled inward in order to progressively increase the clearance and thus reduce the effect of any flow in the gaps on the shear measurements.

The element and the disk are of approximately equal depth, 0.224 and 0.219 in., respectively, and are both made of the same stainless steel stock as the flat plate. The frame and the flexures are made of Invar, which, up to temperatures of 400°F, has a coefficient of thermal expansion of 0.9×10^{-6} in./in.°F, or approximately 1/10 that of mild steel. Total depth of the unit from the top surface of the element to the bottom of the frame is less than 1-1/8 in.

The frame is equipped with an oil dashpot for damping the unit and a soft iron core which constitutes the moving part of a differential transformer used as a position-sensing device (Cf. following section).

The flexures, made of 0.001 in. Invar shim stock, are centrally stiffened as a precaution against buckling since they may be subject to compression stresses during tunnel starting operations.

The transformer coil (Schaevitz coil - Fig. 11) holder with the dashpot elements is connected to the disk by means of two vertical struts and constitutes the fixed part of the unit.

Two locking screws in the frame serve the dual purpose of restricting lateral motion of the balance and locking it in a fixed position for handling purposes. In addition, motion in all three planes is severely restricted by the struts, the disk, and the gap around the element.

The disk with the element was lapped so as to present a continuous smooth surface to the local air flow. For this purpose, the element was held fixed by melting wax in the clearance between the frame and the struts and allowing it to harden.* After the lapping

---

* Use of the locking screws was not made because the degree of tightening required for the lapping operation would have induced large stresses in the flexures.

operation, the wax was dissolved with alcohol and the surface smoothness checked by means of a quartz optical flat. Horizontal alignment of disk and element surfaces was estimated to be within two wave lengths of a monochromatic light source (approximately 0.00003 in.).

The disk is held in the flat plate by means of four sets of concentric "push-pull" screws, permitting horizontal alignment of the surfaces to within 0.0001 in. Grooves are provided for O-ring seals between the disk and the flat plate and around the leveling screws.

The weight of the balance is 17 gm (0.038 lbs.), its spring constant is 50 gm/in., and its natural frequency approximately 33 cps (Cf. Appendix A). The linkage and weight of the chain in the nulling device described below increases the spring constant slightly, but not more than a few per cent.

Two views of the assembled unit are shown in Fig. 12, and its position relative to the flat plate is illustrated in Fig. 13.

4. Position-Sensing Device

Since it is necessary to locate the floating element to within a few microinches, a very sensitive position-sensing device is required. For this purpose, a Schaevitz linear variable differential transformer (Ref. 18) of type 005M-LT was used. This instrument is rated for ambient temperatures up to 550°F and a linear range of ±0.005 in.. It consists of a primary (input) coil, two secondary (output) coils wound so that the induced voltages oppose each other, and a movable iron core. Extremely compact, it has a diameter of 5/16 in. and a length of 3/8 in..

The transformer circuit is shown in Fig. 14. A Hewlett-Packard

low frequency oscillator provides a 1 volt - 25 Kc input to the primary coil, and the signal from the secondary circuit is indicated on a H-P vacuum tube voltmeter (shown at lower right of Fig. 8). A typical signal vs. displacement curve is given in Fig. 15.

5. Chain-Loading Null System

The nulling device makes use of the weight of a jeweler's chain to balance the shear drag on the floating element. The principle is that of the chainomatic balance commonly used in chemical laboratories. It has the inherent advantages of simplicity, continuous force variation, adaptability to remote control, and a wide choice of ranges permitting accurate measurements of very small forces.

The use of chain loading was dependent upon a frictionless means of converting a vertical force (chain weight) into a horizontal restoring force. This was accomplished with a symmetrical w-shaped linkage, the ends of which are fixed to the balance housing, and its center to the frame supporting the floating element, as shown in Figs. 10 and 13. The loading chain is suspended from the apices of the W-linkage (load transfer linkage) so that a variable differential force is obtained by progressively increasing the chain length on one side and decreasing it on the other. The ratio of differential chain load to drag force on the element is dependent on the geometry of the load transfer linkage (Cf. Appendix B).

Initial trials were made with one continuous chain of the flattened type with its center portion looped over a sprocket, the rotation of which provided the required differential loading. However, substantial scatter was encountered in the system. This was traced

to slight displacements of the transfer linkage support points, twisting of the loading chain, and slippage on the sprocket. Elimination of the first was accomplished by cementing the joints, and the second and third, by substituting a chain with oval links (supplied by the Torsion Balance Co., Clifton, N. J.) for the flattened one. The latter necessitated a modification of the actuator system. The chain was split, with its inner ends suspended from two counter weights at the ends of a thin wire wound around an 80-pitch screw, as shown in Fig. 13. The center point of the wire is pinned to the screw in order to prevent slippage, and sufficient windings are provided on either side of the center to allow full travel of the loading chain. The screw is geared to a vertical shaft extending through the bottom of the chain well to an external rotary drive mechanism provided with a flexible pressure seal.* The differential chain load -- and hence the shear drag on the floating element -- is indicated on a dial and counter visible in Fig. 9.

Two important factors required careful investigation: namely, the effect of tunnel vibrations and thermal expansion on the chain and linkage.

Tests made with a dummy balance mounted on the test section housing during tunnel operation proved that the chain was insensitive to the induced vibrations. This was not surprising in view of the fact that the fundamental frequencies of the chain system are of the order of a few cycles per second, and hence, substantially lower than the tunnel frequencies. Moreover, it was observed that the chain had a

---

* The well is vented to the test section by the gap around the floating element.

large damping effect on the balance due to the frequency differential between the two. Full advantage of this fact was taken in that, for most of the experiments, no oil damping was used.

The effect of thermal expansion on loading chain, wire, and screw are negligibly small compared to other sources of error. However, the load transfer linkage may be quite sensitive to temperature, depending upon its geometry and its coefficient of expansion relative to that of the balance housing. Since the geometry of the transfer linkage determines the force ratio (ratio of shear drag on element to differential chain load), it is imperative that any changes in it be very small. A quantitative discussion of the effect of temperature on the force ratio is given in Appendix B, in which it is shown that the induced error for the present operating temperature is conservatively estimated as $\pm\frac{1}{2}\%$.

6. Calibration and Estimated Accuracy of Force Measurements

The method of calibration is illustrated in Fig. 13. A pan is suspended from a single nylon thread passing over a pulley with jewel bearings and attached to the frame of the balance. Thus, the pan loading simulates shear drag on the floating element. Calibration curves for the forward element are given in Fig. 17. The use of two different ranges was made possible by changing the geometry of the load transfer linkage, thus permitting more accurate measurements of laminar skin friction.* For the 400 mg range, repeatability was found to be within 2 mg, and for the 130 mg range, 3/4 mg.

---

* Its adaptibility to variations in total range serves to illustrate the versatility of the present null device.

The turbulent surface shear measurements varied from 180 to 300 mg, and the laminar ones from 20 to 55 mg. The sources of error and a conservative estimate of their magnitude are as follows:

Instrument Scatter	$\pm 1\frac{1}{2}$ - $2\frac{1}{4}\%$ (Turbulent)
	± 3 - $7\frac{1}{2}\%$ (Laminar)
Thermal (transfer linkage)	$\pm \frac{1}{2}\%$
Gap	+3%

No corrections were made for pressure gradients since these were very small if not indeterminable at the higher tunnel reservoir pressures required for the turbulent shear measurements.

The determination of skin friction coefficients is also dependent upon the dynamic pressure and the boundary layer momentum thickness (for turbulent shear). Hence, inaccuracies in the determination of these quantities also affect the final results. However, these sources of error are estimated not to exceed $\pm 1\%$.

III. TRANSITION AND BOUNDARY LAYER STUDIES

A. Flat Plate Flow Characteristics

The flat plate surface pressures and temperatures are shown in Figs. 18, 19, and 20, respectively, for representative reservoir pressures from 47 to 109.4 psia giving a range of Reynolds numbers per inch from 1.07 to 2.50 x 10^5*. As is shown in Fig. 18, the pressure distribution is relatively flat for the first two-thirds of the plate length, followed by a rather severe uniform positive gradient extending to the trailing edge. This gradient is attributed to a fan of waves coming from the nozzle wall. Some attempts were made to eliminate it by reflecting the waves away from the plate surface. While the uniform gradient was cancelled, other equally undesirable pressure non-uniformities resulted. The surface temperatures yield recovery factors of 0.86 to 0.88, thus indicating an essentially-insulated model (Ref. 20). Schlieren photographs of the flow over the flat plate at p_o = 94.4 psia are given in Fig. 21.

The effect of the throat waves mentioned earlier is that of thickening the laminar boundary layer downstream of the interaction, thus leading to a higher effective Reynolds number than that measured from the flat plate leading edge. That similarity exists between the laminar boundary layer upstream and downstream of this interaction is shown by the velocity profiles in Fig. 33, thus indicating that local distortions of the flow are rapidly damped. In the following two

---

* The viscosity-temperature relation used in the computation of Re is that of Hirschfelder, Bird, and Spotz (Ref. 19), since it is considered the most reliable for very low temperatures (Cf. Ref. 16). The ambient temperature for the present experiments is approximately 90°R.

sections the discussion is based on plate (or uncorrected) Reynolds number since the effective Re is unknown; however, this factor imposes no severe restrictions in view of the qualitative nature of most of the laminar results.

B. Transition by Transverse Contamination

Transition by transverse contamination due to the mixing of the turbulent side-wall boundary layer with the laminar boundary layer on a flat plate was first noted by Charters (Ref. 21) in 1939. His experiments performed in low speed flow showed that contamination spread from the plate leading edge at a uniform angle of $9\frac{1}{2}^{\circ}$ independent of speed in the 20 to 60 mph range.* That this phenomenon can be considered a mixing process was suggested by Liepmann in an appendix to Ref. 21. In more recent experimental research in compressible flow, Liepmann, Roshko, and Dhawan (Ref. 23) incidentally noted transverse contamination which spread from the leading edge of a flat plate at an angle of approximately 9° at M = 1.4.

The present experiments at M = 5.8 showed a marked delay in the origin of transverse contamination; it did not occur until stations far downstream from the leading edge of the flat plate were reached. The Reynolds number per inch was varied by changing the tunnel reservoir pressure, and in all cases, transverse contamination was found to originate at Reynolds numbers of approximately 1.5 to 2×10^6 and to spread at a uniform angle of $5\frac{1}{2}^{\circ}$. The former fact, coupled with the

* In a theoretical treatise, Parker (Ref. 22) obtains a contamination angle of $9\frac{1}{4}^{\circ}$; however, his method of analysis is not entirely clear.

results of later findings, appears to indicate greater stability of the laminar boundary layer. In Fig. 22* the luminescent lacquer serves to illustrate the progressive downstream displacement of the origin of transverse contamination over a section of the flat plate (Sta. 13 to 21, inclusive) as the Reynolds number per inch is decreased from 2.15 to 1.07×10^5. In the lower figure the outline of the turbulent side-wall boundary layer is visible with no indication of transverse contamination across the plate surface. Fig. 23 (solid lines) illustrates the method of detecting contamination with the total-head rake. The sharp pressure rise in the lower figure is indicative of contamination crossing the plate surface 13/16 of an inch off the centerline. The gradual rise of all the curves toward the trailing edge is primarily due to the positive pressure gradient in this region. Agreement between the two techniques (lacquer and rake) was found to be quite good.

Subsequent surveys of the side-wall boundary layer at several streamwise stations and $\frac{1}{2}$ to 1 inch above the plate surface revealed it as partially laminar at the lower reservoir pressures -- lower Re/in; however, in all cases, the origin of transverse contamination was found to occur at a substantial distance downstream of transition on the side-wall, thus precluding an obvious explanation for the delay. In addition, at the higher reservoir pressures, the side-wall boundary layer was found to be already fully turbulent near the plate leading edge. Fig. 24 illustrates the growth of the side-wall boundary layer and eventual spread of transverse contamination for Re/in of 2.15, 1.70, and 1.07×10^5.

---

* The narrow white streaks in the figures are due to oil and are not to be confused with the lacquer pattern.

The smaller angle of spread of transverse contamination compared with that for low speed flow is attributed to the large temperature extremes present in the thermal layer in hypersonic flow.* This argument is substantiated by theoretical and experimental work on the effect of temperature variations on the mixing and divergence of free jets. In a theoretical treatise on two-dimensional jet mixing of a compressible fluid, Pai (Ref. 24) predicts greater divergence of the mixing when the jet temperature is higher than that of the surrounding medium, and lesser divergence for lower jet temperatures. Experimental evidence of the more rapid spread of a turbulent jet as its temperature is raised above that of the receiving medium is supplied by the work of Corrsin and Uberoi (Ref. 25).

For the present case, the static temperature through most of the turbulent boundary layer is close to that of the free stream (Cf. Fig. 34), or cold; whereas, through most of the laminar boundary layer, the temperature is close to that of the wall (Cf. Fig. 31), or hot. The ratio of wall to free stream temperature at M = 5.8 is approximately 7. Thus, the present case corresponds to a cooled turbulent jet exhausting into a hot surrounding medium, and therefore, a smaller angle of spread follows.

For the case of M = 1.4 (Ref. 23), no measurable effect of compressibility on the angle of spread was noted, most probably because the effective temperature difference between the laminar and turbulent boundary layers is small, being only 30 to 40%.

---

* This argument was suggested to the writer by Professor H. W. Liepmann.

C. Induced Transition

The results of the investigation of transverse contamination also revealed the conspicuous absence of natural transition at Reynolds numbers in excess of 5×10^6 (Cf. Fig. 23 upper, and Fig. 24). Boundary layer surveys at Reynolds numbers greater than 5×10^6 indicated the onset of transition; however, this region is subject to a severe adverse pressure gradient, and hence, is not representative of uniform flow over a flat plate.

Means of tripping transition artificially were investigated in order to study the effects of disturbances on the flow and the properties of the turbulent boundary layer. Particular emphasis was placed on the method of injecting small amounts of air into the boundary layer through surface holes in the plate. This technique was explored by Fage and Sargent (Ref. 26) as a means of fixing transition by adjusting the rate of injection, and recently used by Coles (Ref. 11) who presents a discussion of the local effect of the jets on the boundary layer.

1. Effect of Local Disturbances

Air was injected into the boundary layer through single orifices along the plate centerline over a range of Reynolds numbers from 10^6 to 3×10^6. The luminescent lacquer revealed what is interpreted as two spiral vortices generated on either side of the air jet, each individually leading to transverse contamination of the boundary layer at a substantial distance downstream of the jet. A typical lacquer pattern is shown in Fig. 25. Pitot surveys in the wake directly behind the jet revealed local separation, and verified the boundary layer as being turbulent in

the region of contamination. That separation occurs in the wake is not surprising in view of the vertical momentum supplied by the jet and vortices, and the very low kinetic energy of the laminar layers close to the plate surface (Cf. Fig. 31). The distance between the jet and the beginning of contamination decreased as the Reynolds number of the point of injection was increased; however, contamination never started at the point of injection over the range investigated. The corresponding Reynolds number increment varied from approximately 1.3×10^6 to 0.65×10^6 as the jet was displaced from a Reynolds number of 1.1×10^6 to 3×10^6, and the included angle of spread of contamination was approximately 10°. From these results immediate contamination from the jets may not be expected at Re below 4 or 5×10^6.

Small rods 0.25 inches long and 0.028 inches in diameter were mounted normal to the surface of the flat plate at Re of 1.1×10^6 and 1.7×10^6 respectively. These proved ineffective in producing transition. The wake of the rods was traced downstream with no sign of transverse contamination of the boundary layer. A lacquer pattern showing the strong initial disturbance which is eventually damped, and the narrow wake downstream is given in Fig. 26.

In Fig. 27 is sketched the wake and transverse contamination induced by the air jets, and the wake with the absence of transverse contamination behind the rods.

2. Effect of Two-Dimensional Disturbances

Variable rates of air were injected into the boundary layer through the row of surface holes $1\frac{1}{2}$ inches behind the leading edge of the plate. Transition was observed to gradually move upstream as the

mass flow injected was increased to 2% of the boundary layer mass defect (m = 2). A further increase in the rate of injection did not measurably decrease the transition Reynolds number* below 2×10^6. The broken lines in Fig. 23 illustrate transition detection with the total-head rake for m = 2. The transition region is given by the initial sloping part of the curve extending from a Re of about 10^6 to 2×10^6. That the solid line overshoots the broken line beyond Sta. 20 in the lower figure indicates that the turbulent boundary layer resulting from sidewall contamination is thinner than that induced by the air jets.

The corresponding lacquer pattern is shown in Fig. 28 in which can be observed the wake of each individual jet and eventual transition across the plate surface. At the higher reservoir pressures it was also possible to detect transition from local rises in the surface pressure along the flat plate (Cf. Fig. 29). The pressure peaks are associated with the end of the transition region. In his measurements on a flat plate, Coles (Ref. 11) found that these peaks occur slightly downstream of the point of maximum surface shear. Fig. 29 shows that, for a Re/in. of 2.5×10^5, there is already no appreciable change in the pressure rise, and hence Re_T, as m is increased from 1.3 to 1.9.

Distributed surface roughness and single wire trips proved ineffective in hastening transition. In particular, the only effect of a wide, coarse sandstrip (50 grit Emery paper) on the tunnel side wall at a p_o of 47 psia was to thicken the laminar boundary layer.

The transition Reynolds number (Re_T) is here defined as that where a fully turbulent boundary layer is obtained.

D. Boundary Layer Characteristics

During the course of the present investigation a large number of boundary layer surveys were made. The ones presented below are considered typical of the laminar and turbulent boundary layers at M = 5.8.

Measurements of impact pressure, static pressure, and total temperature (i.e., total energy) distributions in the boundary layer completely determine the velocity profile. The present surveys were made with a pitot probe. Sample static pressure surveys through the boundary layer indicated a maximum variation only slightly greater than 1%, thus verifying the near constancy of the pressure. Hence, the surface pressure on the plate was taken as that prevailing throughout the boundary layer. In lieu of total temperature measurements, the conservation of energy equation was used with a Prandtl number correction (Pr = 3/4) whereby conditions in the free stream and on the plate surface (T_w) were satisfied. Actually, the profiles thus obtained varied little from those resulting from the assumption of Pr = 1 (iso-energy). The parameter the most sensitive to variation in total energy through the boundary layer is the momentum thickness θ; however, it is estimated that the error induced by the above assumption does not exceed a few per cent.

Typical impact pressure distributions in a laminar and a turbulent boundary layer at M = 5.8 are shown in Fig. 30.

1. Laminar Boundary Layer

Profiles of velocity, Mach number, density, and temperature for a typical laminar boundary layer on an insulated flat plate are given in Fig. 31. Mass and momentum defect distributions are given in Fig. 32.

The conventional dimensionless parameter $(y/x)\sqrt{Re}$ was not used since the actual Re is unknown. δ, δ^*, and θ are much larger than the theoretical values based on Reynolds number measured from the leading edge. This fact is due to the interaction of the throat waves with the boundary layer on the flat plate (Cf. Sections II.B.1 and III.A). It was, hence, necessary to define the profiles in terms of the local properties of the boundary layer. The choice of y/θ was made because $(\theta/x)\sqrt{Re}$ varies little with Mach number and is of order unity. The wall slope of the velocity profile was obtained from local surface shear measurements discussed in Section IV.

The velocity profile is almost linear as originally predicted by von Karman and Tsien (Ref. 27). That the hypersonic boundary layer is so clearly defined physically can be partly explained from consideration of the viscous dissipation $\mu(\partial u/\partial y)^2$. While the viscous dissipation becomes small near the edge of the boundary layer, a large velocity gradient $\partial u/\partial y$ can be sustained since the viscosity (or temperature) drops rapidly to its relatively low free stream value. The viscosity drops by almost a factor of 10 from the wall to the edge of the boundary layer. The theoretical boundary layer Mach number distribution given by Van Driest (Ref. 28) for a free stream Mach number of 6, when converted from $y/x\sqrt{Re}$ to y/θ^*, is in excellent agreement with the present experimental results. Van Driest utilizes the Crocco method of solution of the boundary layer equations assuming a Prandtl number of 3/4 and the Sutherland formula for viscosity. The large density gradient near the edge of the laminar boundary layer (Cf. Fig. 31) appears as the dark

---

* From Ref. 29, for $M = 6$ and $T_\infty = 100^\circ R$, $\theta/x\sqrt{Re} = 0.66$.

line above the flat plate in the schlieren pictures of Fig. 21.

A comparison of experimental velocity profiles with the theoretical profiles of Young and Janssen (Ref. 29) is given in Fig. 33. Young and Janssen present distributions of flow parameters in the compressible laminar boundary layer for a very low ambient temperature (100°R) comparable to that obtained in the present experiments (approximately 90°R), whereas the theoretical profiles of Crocco, (Ref. 30), Van Driest (Ref. 28), and others are restricted to much higher ambient temperatures within the range of validity of their assumptions. The temperature effect is pronounced. For instance, at M = 5.8, $(\delta/x)\sqrt{Re}$ is approximately 15 for an ambient temperature of 400°R, while it is 20 for 100°R (Cf. Ref. 29).

The characteristic parameters of the laminar boundary layer are listed in Table I. It is to be noted that the displacement thickness is almost 3/4 of the boundary layer thickness due to the very low mass flow in the laminar layer.

An extensive survey of theoretical literature on the compressible laminar boundary layer is given by Kuerti in Ref. 31 and also by Bradfield, DeCoursin, and Blumer (Ref. 14).

2. Turbulent Boundary Layer

Profiles of velocity, Mach number, density, and temperature for a typical turbulent boundary layer on an insulated flat plate at M = 5.8 are given in Fig. 34. Mass and momentum defect distributions are given in Fig. 35. The turbulent boundary layer is characterized by an almost linear density profile which appears as a region of uniform light intensity

through a schlieren system (Cf. nozzle wall in Fig. 21). A comparison of turbulent velocity profiles with power law profiles is given in Fig. 36. The experimental profiles for R_θ of 3430 and 4040 follow very closely the 1/7th power law as was also noted for a turbulent velocity profile at a Mach number of 7 by Wegener, Winkler, and Sibulkin at NOL (Ref. 32).

Fig. 37 shows a velocity profile at M = 5.8 with profiles obtained by Coles at Mach numbers of 2.6, 3.7, and 4.5, in a coordinate system based on a formulation of similarity in compressible turbulent boundary layers proposed by Coles (Ref. 11). The parameter ρ_r in Fig. 37 is a pseudo-density chosen arbitrarily to give agreement with incompressible data. The value of ρ_r/ρ_w is 1.81 for the velocity profile at M = 5.8.

In Table II is given a list of experimentally obtained turbulent boundary layer parameters at M = 5.8 and the corresponding calculated values for 1/5th and 1/7th power profiles obtained by Tucker (Ref. 33). The agreement between the experimental parameters for R_θ of 3430 and 4040 with those obtained from the 1/7th power law is noteworthy. The skin friction results given in Table II are discussed in Section IV.

A good review and comparison of the theoretical literature on the compressible turbulent boundary layer is presented in Ref. 11. Literature surveys are also given in Refs. 14 and 34.

E. Discussion

Of particular interest in this investigation is the delay of natural transition to Reynolds numbers in excess of 5×10^6 and the apparent inability of artificial disturbances and the sidewall boundary

layer to induce transition at Reynolds numbers much below 2×10^6. Although the present work is in the nature of an exploratory investigation of transition in hypersonic flow, it offers an insight into the phenomenon.

Several reasons may be advanced for the existence of extensive laminar layers. It is reasonable to expect a very low turbulence level* in hypersonic wind tunnels because of the large contraction from the settling chamber to the throat and the large acceleration of the flow. Because of its narrowness, one may visualize the throat as a filter which prevents passage of large flow eddies. Thus, one may expect the flow in the test section to be relatively insensitive to conditions in the settling chamber. In support of this argument, Laufer (Ref. 35) recently found that a change in turbulence level by a factor of 10 in the settling chamber of the JPL 20" supersonic wind tunnel did not measurably affect transition on a model in the test section at Mach numbers above 2.5.

However, the persistence of the boundary layer to remain laminar far downstream of artificial disturbances leads one to suspect either a greater inherent stability of the layer, or a very low rate of amplification of induced velocity fluctuations, or both. In particular, the wave length of propagation of small disturbances in the laminar layer may become very large at high Mach numbers ($\lambda \backsim \delta \backsim M^2$). Since a finite

---

* Turbulence level is defined as follows:

$$\sigma = 100 \frac{\sqrt{(\overline{u'^2} + \overline{v'^2} + \overline{w'^2})\frac{1}{3}}}{U}$$

or

$$\sigma = 100 \sqrt{\overline{u'^2}} / U \qquad \text{for isotropic turbulence where}$$

$\sqrt{\overline{u'^2}}$ etc. are r.m.s. values of velocity fluctuations and U is the mean flow velocity.

number of wave lengths is required for these disturbances to become large enough to cause the breakdown of laminar motion, a substantial delay can be expected before transition occurs.*

Van Driest's calculations based on the Lees-Lin theory show a progressively decreasing critical Reynolds number (Re_{crit}) with increasing Mach number on an insulated flat plate (Cf. Introduction). That Re_{crit} becomes very small at high Mach numbers -- at M = 5, Van Driest obtains $Re_{crit} < 200$ -- might be questioned in light of the present results. But transition is also dependent on wave lengths and amplification rates for which there are presently no calculations. It should be noted, however, that the Lees-Lin theory is not strictly valid at high Mach numbers. Hence, there is need for extensive experimental and theoretical work in the field of stability and transition at high Mach numbers.

The trend of transition with Mach number is shown in Fig. 38. The data for Mach numbers from 2 to 4.5 were obtained in the JPL 20 in. wind tunnel (Ref. 11). The transition region is defined by curves representing respectively a minimum and a maximum in surface shear. While quantitatively the transition Reynolds number (upper curve) is dependent upon the effects of the given wind tunnel, qualitatively it is significant that the transition region increases to higher Reynolds numbers in the higher supersonic regime.

The present results and those of Coles (Ref. 11) indicate that artificial disturbances become progressively less effective in stimulating

---

* This argument was suggested to the writer by Professor Lester Lees.

transition as the Mach number is increased. In particular, the small effect of surface roughness at high Mach numbers suggests that a smooth surface is not as essential as in low speed flow for the existence of extensive laminar layers. Of the various artificial disturbances, air injection proved to be the most effective transition tripping device. It also offers the advantage of control. This feature was fully exploited in the skin friction investigation discussed in Section VI.

IV. SKIN FRICTION MEASUREMENTS

The flow characteristics over the flat plate are essentially the same as those for the transition studies. The shear measurements in the transition region and in a fully developed turbulent boundary layer were obtained by inducing transition with air injection.

The skin friction data presented here were obtained with the forward surface element (Sta. 15.5). Unfortunately, the rear element (Sta. 23) was subject to streamwise and spanwise pressure gradients (Cf. Figs. 18 and 19), thus precluding any reliable interpretation of data. While slight streamwise pressure gradients were present over the forward element at low reservoir pressures (Cf. Fig. 18, p_o's of 47 and 59.4 psia), the flow was relatively uniform at the higher reservoir pressures which were required to obtain a fully developed turbulent boundary layer at Sta. 15.5. The effect of a pressure gradient on surface shear at M = 5.8 is discussed in Appendix C.

Some attempt was made to determine the effect of small changes in balance chamber pressure on measured turbulent shear. The pressure was varied over a range of $\pm 10\%$ of equilibrium with the external flow over the flat plate, by means of a controlled leak, and by pumping down the chamber, respectively. No measurable change in shear was noted either way when the chamber pressure was within a few per cent of equilibrium. A 10% increase in pressure resulted in a small percentage drop in shear. From the foregoing, it is estimated that any error in shear measurements due to existing leakage into the balance chamber is negligible.

The Reynolds number (uncorrected) at the forward surface element

was varied from approximately 10^6 to 4×10^6 by proportionately varying the reservoir pressure.

A. Effect of Variable Air Injection on Shear

Surface shear measurements were made for variable rates of air injection through the row of surface holes near the leading edge. The results are shown in Fig. 39 where each curve represents a fixed Reynolds number at the element station, i.e., a fixed reservoir pressure. For each condition transition was progressively moved upstream across the element by increasing the intensity of the air jets. The jet mass flow is expressed as a percentage of the mass defect in the boundary layer (m).

The measurements for m = 0 (no induced disturbance) indicate laminar shear over the whole range of Reynolds numbers. The finite amount of injection (m = 0.065) required to bring the onset of transition over the element at Re of 3.9×10^6 shows that natural transition must occur at a substantial distance downstream of this point, in support of previous results discussed in Section III. It is also shown in Fig. 39 that, in spite of large rates of air injection, a fully developed turbulent boundary layer is not obtained at Reynolds numbers below 2×10^6. The lower four curves (Re 1.2 to 1.9×10^6) show an almost random rise in surface shear with no indication of eventual flattening as is the case for the upper curves ($Re > 2 \times 10^6$). It is interesting to note that air injection has no measurable effect on surface shear up until the onset of transition, with the exception of the lower two curves in Fig. 39 (Re 1.2 and 1.4×10^6) where the initial decrease in

surface shear is indicative of extensive separation behind the jets, followed by laminar reattachment.

The rapidly increasing rate of air injection required to trip transition as the Reynolds number is reduced below 4×10^6 indicates that the mechanism of transition is essentially the same as in low speed flow. The intensity of the induced disturbance must be substantially magnified in order to accelerate instability of laminar waves.

In Fig. 40 is shown the variation of skin friction coefficient with Reynolds number. The transition curves shown correspond to different rates of air injection; however, they are not true transition curves since the data for each Reynolds number were obtained under different operating conditions (x fixed, Re/in variable). Here it is clearly shown that fully turbulent shear is only obtained down to a Reynolds number of 2.3×10^6 with $m \geq 2.5$. While the effective Reynolds numbers of the experimental data are unknown, Fig. 40 offers some measure of comparison with the incompressible predictions of von Karman (Ref. 36) and Coles (Ref. 11, Table I).

The consistently low values of laminar skin friction compared with measurements at lower speeds and reasonable theoretical predictions (Refs. 28, 29, 30, etc.) are indicative of a higher effective Reynolds number than that measured from the leading edge of the flat plate (uncorrected Re). This is in agreement with the results of boundary layer surveys discussed in Section III. The scatter in the laminar measurements as shown in Fig. 40 is relatively large, and hence, with the additional uncertainty of the effective Reynolds number, the laminar data are of qualitative interest only. By contrast, the turbulent

measurements were repeatable within a few per cent.

B. Local Turbulent Skin Friction

While an element of uncertainty enters the determination of the effective free stream Reynolds number associated with turbulent skin friction measurements, the local shear for a fully developed turbulent boundary layer may be uniquely described in terms of local flow properties, in particular the Reynolds number based on momentum thickness, R_θ. A full discussion of the interpretation of turbulent shear data is given by Coles (Refs. 11 and 37).

In Fig. 41 are presented the present turbulent skin friction data ($m = 2.8$) at $M = 5.8$ in terms of R_θ. The corresponding velocity profiles are given in Fig. 36, and the boundary layer parameters in Table II. The measurements of Coles (Ref. 11) and Hakkinen (Ref. 13) on a flat plate, and Chapman and Kester (Ref. 9) on a cylinder serve to illustrate the effect of Mach number on turbulent skin friction. No correction for cylinder curvature was applied to the data of Chapman and Kester since it is estimated to be very small. The broken lines in Fig. 41 representing their results are subject to any error presently made in reducing their measurements of mean friction and Re to corresponding values of local friction and R_θ. For this purpose the following relations were used,

$$C_F = 2R_\theta/Re \qquad \text{or} \qquad R_\theta = \tfrac{1}{2}Re\, C_F \tag{IV-1}$$

from whence

$$C_f = 2\,dR_\theta/dRe = C_F - Re \left| dC_F/dRe \right| \tag{IV-2}$$

The incompressible reference chosen for Fig. 41 is that of Coles (Ref. 11, Table I) since it offers very good agreement with low speed experimental data for Re $> 10^6$ (Cf. Fig. 8 of Ref. 13 and Figs. 1 and 2 of Ref. 11).

As shown in Figs. 39 and 40, the maximum value of C_f observed was approximately 0.00130. Values of C_f at Reynolds numbers below 2.3×10^6 (or $R_\theta < 2500$ in Fig. 41) were lower. Hence, in the present measurements at M = 5.8 turbulent shear was not obtained below an R_θ of approximately 2,500. The lower limit observed by Coles in supersonic flow was 2,000 and the turbulent shear measurements of Hakkinen at M = 1.5 extended to values of R_θ down to 1,600. This clearly illustrates the trend of turbulent boundary layer development toward larger values of R_θ with increasing Mach number, as was first noted and discussed by Coles (Ref. 37).

The variation of experimental local turbulent skin friction with Mach number is shown in Fig. 42 for $R_\theta = 4{,}000$ and $C_f/C_{fi} = R_\theta/R_{\theta i}$ respectively. The latter closely approaches a constant Reynolds number, which, from the incompressible reference and the data of Coles and Chapman and Kester, is estimated to lie between 5 and 6×10^6. Measurements in high speed flow of other investigators (Cf. Refs. 13, 14, 38, etc.) are not included in Fig. 42 because either R_θ could not be deduced, or their data are not within the R_θ range of the present results. In particular, the skin friction values of Lobb, Winkler, and Persh (Ref. 38) at M = 5, 6.8, and 7.8 cover a higher range of values of R_θ than the present measurements, and, aside from substantial heat

transfer, they are generally low compared with the present direct measurements and those of Coles. Their results were deduced from boundary layer surveys and measurements of heat transfer rates. Nevertheless, Lobb et al contribute much useful information on the characteristics of the hypersonic turbulent boundary layer.

Finally, it is shown that, over the R_θ range presently investigated, C_f/C_{fi} is relatively constant, since it is approximately 0.40 for constant R_θ, and 0.46 for C_f/R_θ constant (Cf. Table II).

V. CONCLUSION

The results of the present transition and skin friction investigation on an insulated flat plate at Mach 5.8 indicate the following:

(1) A very high transition Reynolds number (in excess of 5×10^6 in the present case) and the inability of various disturbances to trip transition at low Reynolds numbers, which appears to indicate greater stability of the laminar boundary layer in hypersonic flow than at lower speeds.

(2) A delay in the origin of transverse contamination triggered by the side-wall boundary layer, and a $5\frac{1}{2}^\circ$ angle of spread (compared with contamination originating at the leading edge and spreading at an angle of $9\frac{1}{2}^\circ$ in low speed flow).

(3) Evidence that air injection into the boundary layer is a more effective means of tripping transition at hypersonic speeds than the conventional devices used in low speed flow (wire and fence trips, surface roughness, etc.).

(4) Qualitative evidence that the mechanism of transition does not differ from that of lower speed flows (Tollmien-Schlichting oscillations).

(5) A verification of the theoretically predicted laminar boundary layer profiles at a hypersonic Mach number.

In addition direct measurement of turbulent skin friction has been extended to Mach 5.8, and indicates a continued decrease of coefficient with increasing Mach number.

In light of the present findings, the following suggestions for

future experimental research are advanced:

(1) A comprehensive investigation of the stability of the laminar boundary layer in high speed flow with controlled-frequency disturbances, such as that performed by Schubauer and Skramstad in low speed flow. Hot wire measurements of wave lengths and amplification rates of laminar disturbances are particularly important.

(2) An investigation of transition Reynolds number variation with Mach number with particular emphasis on the range from Mach 3 to hypersonic speeds. A hypersonic wind tunnel with a flexible nozzle permitting continuous Mach number variation would be particularly well suited for this work.

(3) An investigation of the variation of contamination angle with Mach number.

REFERENCES

1. Gazeley, Carl, Jr., "Boundary Layer Stability and Transition in Subsonic and Supersonic Flow", JAS, Vol. 20, No. 1, January 1953.

2. Czarnecki, K. R., and Sinclair, A. R., "Factors Affecting Transition at Supersonic Speeds", NACA RM L53I18a, November 1953.

3. Lange, A. H., Gieseler, L. P., and Lee, R. E., "Variation of Transition Reynolds Number with Mach Number", JAS, Vol. 20, No. 10, October 1953, Readers' Forum.

4. Schubauer, G. B., and Skramstad, H. K., "Laminar Boundary Layer Oscillations and Transition on a Flat Plate", NACA WTR W-8, ACR, April 1943.

5. Dryden, H. L., "Some Recent Contributions to the Study of Transition and Turbulent Boundary Layers", NACA TN No. 1168, April 1947.

6. Lees, Lester, and Lin, C. C., "Investigation of the Stability of the Laminar Boundary Layer in a Compressible Fluid", NACA TN No. 1115, September 1946.

7. Lees, Lester, "The Stability of the Laminar Boundary Layer in a Compressible Fluid", NACA TN No. 1360, 1947.

8. Van Driest, E. R., "Calculation of the Stability of the Laminar Boundary Layer in a Compressible Fluid on a Flat Plate with Heat Transfer", North American Aviation Report No. AL-1334, September 1951, or JAS, Vol. 19, No. 12, December 1952.

9. Chapman, D. R., and Kester, R. H., "Measurements of Turbulent Skin Friction on Cylinders in Axial Flow at Subsonic and Supersonic Velocities", JAS, Vol. 20, No. 7, July 1953.

10. Li, T. Y., and Nagamatsu, H. T., "Effect of Density Fluctuations on the Turbulent Skin Friction on a Flat Plate at High Supersonic Speeds", JAS, Vol. 18, No. 10, October 1951, Readers' Forum.

11. Coles, D. E., "Measurements in the Boundary Layer on a Smooth Flat Plate in Supersonic Flow, California Institute of Technology, Ph.D. Thesis, June 1953, also JPL Reports No. 20-69, 20-70, and 20-71 (in press).

12. Dhawan, Satish, "Direct Measurements of S_K in Friction", California Institute of Technology, Ph.D. Thesis, June 1951, also NACA TN No. 2567, January 1952.

13. Hakkinen, R. J., "Measurements of Skin Friction in Turbulent Boundary Layers at Transonic Speeds", California Institute of Technology, Ph.D. Thesis, June 1954.

14. Bradfield, W. S., De Coursin, D. G., and Blumer, C. B., "Characteristics of Laminar and Turbulent Boundary Layers at Supersonic Velocity", University of Minnesota, Research Report 83, July 1952.

15. Buhler, R. D., "Condensation of Air Components in Hypersonic Wind Tunnels -- Theoretical Calculations and Comparison with Experiment", Contract No. DA-04-495-Ord-19, California Institute of Technology, Memorandum No. 13, December 1, 1952.

16. Eimer, Manfred, "Direct Measurement of Laminar Skin Friction at Hypersonic Speeds", California Institute of Technology, Ph.D. Thesis, June 1953, also Hypersonic Wind Tunnel Memorandum No. 16, California Institute of Technology.

17. Stalder, J. R., and Slack, E. G., "The Use of a Luminescent Lacquer for the Visual Indication of Boundary Layer Transition", NACA TN No. 2263, January 1951.

18. Schaevitz, H., "The Linear Variable Differential Transformer", Proceedings of the Society for Experimental Stress Analysis, Vol. 4, No. 2, 1947.

19. Hirschfelder, J. O., Bird, R. B., and Spotz, E. L., "Viscosity and Other Physical Properties of Gases and Gas Mixtures", ASME Transactions, p. 921, November 1949.

20. DeLauer, R. D., "Experimental Heat Transfer at Hypersonic Mach Number", California Institute of Technology, Ph.D. Thesis, June 1953, also Hypersonic Wind Tunnel Memorandum No. 14, California Institute of Technology.

21. Charters, A. C., Jr., "Transition between Laminar and Turbulent Flow by Transverse Contamination", NACA TN No. 891, March 1943.

22. Parker, E. N., "The Concept of Physical Subsets and Application to Hydrodynamic Theory", University of Utah and U.S. NOTS, Inyokern, 21 November 1952, Salt Lake City, Utah; p. 168, "Angle of Diffusion of Jets".

23. Liepmann, H. W., Roshko, A., and Dhawan, S., "On Reflection of Shock Waves from Boundary Layers", NACA TN No. 2334, April 1951, p. 23 and Fig. 18.

24. Pai, S. I., "Two-Dimensional Jet Mixing of a Compressible Fluid", JAS, Vol. 16, No. 8, August 1949.

25. Corrsin, S., and Uberoi, M. S., "Further Experiments on the Flow and Heat Transfer in a Heated Turbulent Jet", NACA TR No. 998, 1950; also NACA TN No. 1865, 1949.

26. Fage, A., and Sargent, R. F., "An Air-Injection Method of Fixing Transition from Laminar to Turbulent Flow in a Boundary Layer", British ARC, R & M 2106, June 1944.

27. von Karman, Th., and Tsien, H. S., "Boundary Layer in Compressible Fluids", JAS, Vol. 5, No. 6, April 1938.

28. Van Driest, E. R., "Investigation of Laminar Boundary Layer in Compressible Fluids Using the Crocco Method", NACA TN No. 2597, January 1952.

29. Young, G. B. W., and Janssen, Earl, "The Compressible Boundary Layer", JAS, Vol. 19, No. 4, April 1952.

30. Crocco, Luigi, "The Laminar Boundary Layer in Gases", North American Aviation, Inc., APL/CF-1038, Report AL-684, July 1948 (translation).

31. von Mises, Richard, and von Karman, Th., "Advances in Applied Mechanics", Vol. 2, Academic Press Inc., 1951.

32. Wegener, P. P., Winkler, Eva M., and Sibulkin, M., "A Measurement of Turbulent Boundary Layer Profiles and Heat Transfer Coefficient at M = 7", JAS, Vol. 20, No. 3, March 1953, Readers' Forum.

33. Tucker, Maurice, "Approximate Calculation of Turbulent Boundary Layer Development in Compressible Flow", NACA TN No. 2337, April 1951.

34. Rubesin, M. W., Maydew, R. C., and Varga, S. A., "An Analytical and Experimental Investigation of the Skin Friction of the Boundary Layer on a Flat Plate at Supersonic Speeds", NACA TN No. 2305, February 1951.

35. Laufer, John, "Factors Affecting Transition Reynolds Numbers on Models in Supersonic Wind Tunnels", JAS, Readers' Forum (to be published).

36. von Karman, Th., "Turbulence and Skin Friction", JAS, Vol. 1, No. 1, 1934.

37. Coles, D. E., "Measurements of Turbulent Friction on a Smooth Flat Plate in Supersonic Flow", JAS (to be published).

38. Lobb, R. K., Winkler, Eva, and Persh, Jerome, "Experimental Investigation of Turbulent Boundary Layers in Hypersonic Flow", paper presented at the 22nd annual meeting of the IAS, January 25-29, 1954, IAS Preprint No. 452.

APPENDIX A

SPRING CONSTANT OF THE BALANCE UNIT

In view of the geometry of the flexures and the very small displacements of the system, the simple beam theory adequately predicts the deflection under load. For a centrally stiffened flexure with rigid end supports, the end deflection is given by the following equation:

$$y = FL/W \left[1 - \alpha \tanh \delta/\alpha - (1 - \delta) \operatorname{sech} \delta/\alpha \right] \qquad (A\text{-}1)$$

where

$$\alpha = \frac{2 \sqrt{EI/W}}{L}$$

and the notation is as follows (Cf. Fig. A1):

W	weight of the balance
F	applied shear force
L	length of flexure
δ	non-dimensional total length of unstiffened part of flexure ($\delta = 1$ with no stiffener)
I	moment of inertia of flexure about axis normal to plane of motion
E	modulus of elasticity of flexure material

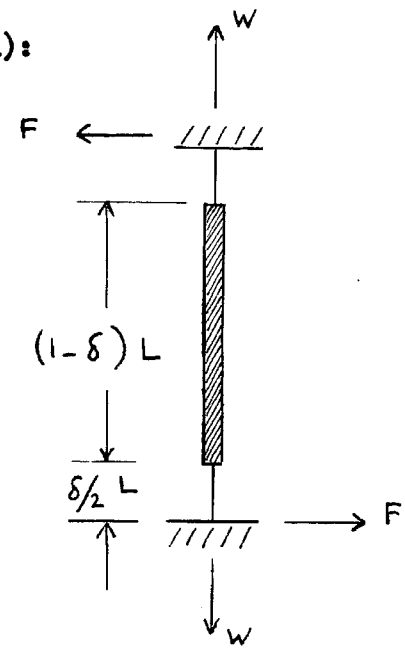

Fig. A1

The spring constant, or applied force per unit deflection, is thus,

$$k = F/y = W/L \left[1 - \alpha \tanh \delta/\alpha - (1 - \delta) \operatorname{sech} \delta/\alpha \right]^{-1} \qquad (A\text{-}2)$$

It may be observed that, for $\delta = 1$, Eq. A-2 reduces to that for an unstiffened flexure

$$k = W/L \left[1 - \alpha \tanh 1/\alpha\right]^{-1}$$

and, as the flexure stiffness becomes vanishingly small, i.e., as α approaches zero, the equation degenerates to

$$k = W/L$$

or the spring constant for small deflections of a simple pendulum.

Since Eq. A-2 was derived with the assumption of rigid end fixity which is never achieved in actual practice, an effective flexure length is determined in conformity with structures' convention, and denoted below by the subscript "e". The parameters for the present balance are the following:

$W = 0.038$ lbs. (17 gms)

$L_e = 0.657$ in.

$\delta_e = 0.714$

$EI = 65.7$ lb.-in.^{2} (2 flexures)

From Eq. A-2, the balance spring constant is calculated to be $k = 49$ gm/in. (the experimentally measured value was approximately 50 gm./in.). The corresponding natural frequency is

$$\omega = \sqrt{gk/W} = 33 \text{ cycles per second}$$

Note: Without stiffeners, the spring constant would have been 43 gm./in., and for an equivalent pendulum, 34 gm./in. (with the actual length of $\frac{1}{2}$ in.); thus, the spring constant for the stiffened flexure configuration used is only about 50% higher than that for the ideal simple pendulum.

APPENDIX B

FORCE RATIO AND ITS VARIATION WITH TEMPERATURE

The force ratio (ratio of shear drag on the floating element to differential chain load) is determined as a function of the geometry of the load transfer linkage from equilibrium of forces and moments (Cf. Fig. B1),

$$f = F_{\tau}/F_c = \xi(1-\xi)/\eta \qquad \text{(B-1)}$$

with the following notation

F_{τ}	shear drag on floating element
F_c	differential chain load
ξ, η	non-dimensional lengths as shown in Fig. B1

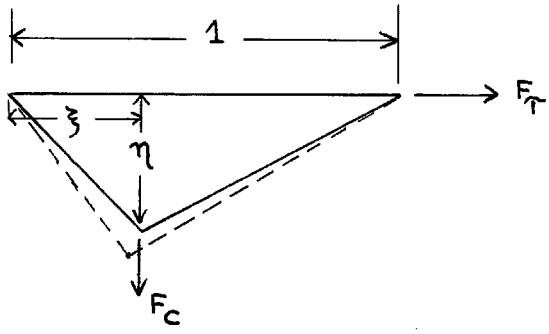

Fig. B1

The possible combinations of ξ and η for a desired force ratio f are given in Fig. 16.

With a temperature rise, differential expansion between the balance housing and the linkage produces a change in its geometry as illustrated by the broken line in Fig. B1. The ensuing change in force ratio is obtained as follows:

$$\left|\frac{\Delta f}{f}\right| = \left(\frac{f^2 - 3f\eta + 1}{f\eta}\right)\varepsilon + 0(\varepsilon^2) \qquad \text{(B-2)}$$

where f and η are the initial values, and

$\varepsilon = \Delta T \, \Delta C$ is the differential elongation per unit length

ΔT (^{o}F) the change in temperature

ΔC (in./in.-^{o}F) the difference in thermal expansion coefficients of balance housing and linkage

Eq. B-2 is plotted in Fig. 16 for various values of f, ξ, and η (second order terms are neglected, since $\varepsilon \ll 1$).

For the present case, f is less than 1 (actually it ranges from about 1/3 to 9/10), and ξ is between 3/8 and 1/2; hence, from Fig. 16,

$$\left| \Delta f/f \right| < 5 \varepsilon$$

The model temperatures are about 150 to 170^{o}F; hence ΔT is approximately 100^{o}F (room temperature reference), and Δc is conservatively estimated as 10×10^{-6} in./in.^{o}F; therefore

$$\left| \Delta f/f \right| < 0.005$$

Hence, the ensuing error in force measurements due to thermal effects on the load transfer linkage is at most $\pm \frac{1}{2}\%$.

APPENDIX C

EFFECT OF PRESSURE GRADIENT ON C_f AT M = 5.8

The momentum-integral relation for two-dimensional flow with a pressure gradient over a flat plate is

$$C_f = \frac{\tau_w}{q_\infty} = 2\frac{d\theta}{dx} - (2 - M_\infty^2 + H)\frac{\theta}{q_\infty}\frac{dP}{dx} \qquad (C\text{-}1)$$

Since the flow in the free stream is essentially isentropic, one can invoke the relation

$$q_\infty = \frac{\gamma}{2} P_\infty M_\infty^2$$

Hence, Eq. C-1 can be written as

$$C_f = 2\frac{d\theta}{dx} + \frac{2}{\gamma}\left(1 - \frac{2 + H}{M_\infty^2}\right)\frac{\theta}{P_\infty}\frac{dP}{dx} \qquad (C\text{-}2)$$

The present experiments at M = 5.8 yield a shape parameter H of approximately 21 for a laminar boundary layer, and 16 for a turbulent one, so that

$$C_f \doteq 2\frac{d\theta}{dx} + K\frac{\theta}{P_\infty}\frac{dP}{dx} \qquad (C\text{-}3)$$

where K = 0.45 (laminar)

0.66 (turbulent)

While $d\theta/dx$ would be affected by a pressure gradient, the major change in surface shear comes from the second term in Eq. C-3.

For example, representative values of momentum thickness and

skin friction coefficients are (Cf. Tables I and II)

	θ(in.)	C_f
Laminar	0.010	3×10^{-4}
Turbulent	0.016	12×10^{-4}

If a pressure gradient ($\frac{1}{P_\infty} \frac{dP}{dx}$) of 1% per inch is assumed, its contribution to surface shear and the percentage change are respectively

	ΔC_f	$\Delta C_f/C_f$ (%)
Laminar	0.45×10^{-4}	15
Turbulent	1.05×10^{-4}	9

For the present skin friction measurements, the pressure gradients over the forward surface element are substantially below 1% per inch, and hence, the possible error in neglecting their effect is within a few per cent.

TABLE I

LAMINAR BOUNDARY LAYER PARAMETERS

$M = 5.8$; $P_o = 94.4$ psia; $T_o = 225^\circ F$

$Re/in. = 2.15 \times 10^5$; $T_\infty = 88^\circ R$

θ (in.)	δ^* (in.)	H	δ^*/δ ‡	R_θ	$C_f \times 10^{-4}$
.00377	.0801	21.2	0.728	810	
.00448	.0841	19.8	0.697	964	
.00839	.1777	21.1	0.787	1800	
.01018	.2088	20.5	0.720	2190	2.5
Young & Janssen (Ref. 29) $M = 5.8$; $T_\infty = 100^\circ R$		24.5	0.810		

‡ δ based on $u/u_\infty = 0.995$ for both measurements and Ref. 29

TABLE II

TURBULENT BOUNDARY LAYER PARAMETERS[1]

$M = 5.8$; $T_o = 225^{\circ}F$

P_o (psia)	M	$Re/in \times 10^{-5}$ (in^{-1})	θ (in.)	R_θ	δ^* (in.)	θ/δ	δ^*/δ	H	$C_f \times 10^{-4}$	C_f/C_{fi} [11]	C_f/C_{fi} [111]
64.4	5.787	1.468	.01688	2477	.2380	.0375	.529	14.10	13.16	0.403	0.467
74.4	5.770	1.697	.01638	2780	.2356	.0361	.519	14.38	12.75	0.400	0.463
94.4	5.792	2.151	.01594	3429	.2500	.0357	.561	15.68	12.23	0.400	0.463
109.4	5.805	2.489	.01623	4040	.2562	.0355	.561	15.79	11.79	0.397	0.462
	5.80					.0340	.546	16.08	-- 1/7th Power Law (Ref. 33)		
	5.80					.0365	.610	16.70	-- 1/5th Power Law (Ref. 33)		

[1] turbulent boundary layer obtained with air jets (m = 2.8)
[11] for $R_\theta = R_{\theta i}$ and C_{fi} from Table I, Ref. 11
[111] for $C_f/C_{fi} = R_\theta/R_{\theta i}$ from Table I, Ref. 11

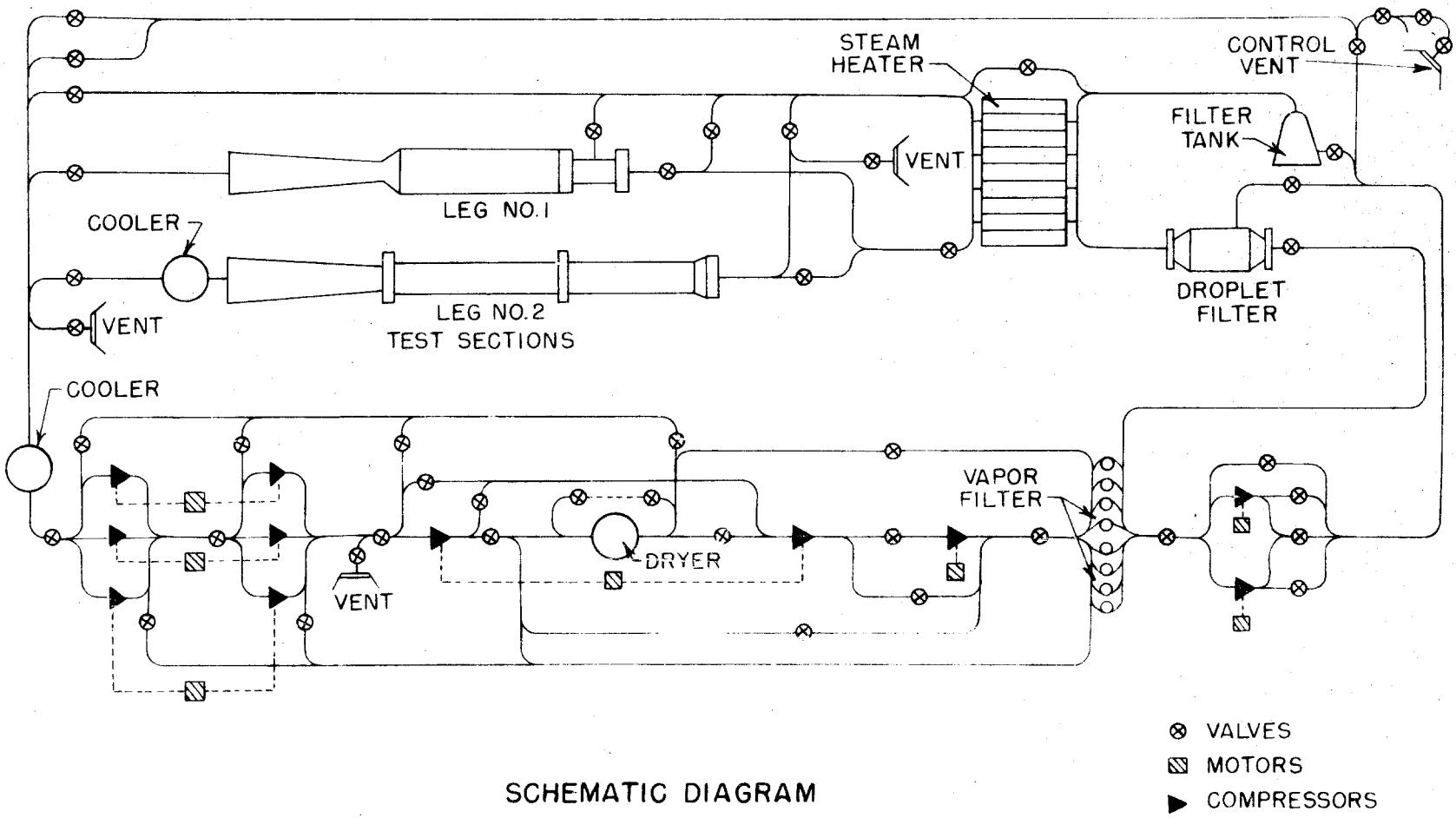

SCHEMATIC DIAGRAM

OF GALCIT 5x5in. HYPERSONIC WIND TUNNEL INSTALLATION

FIG 1

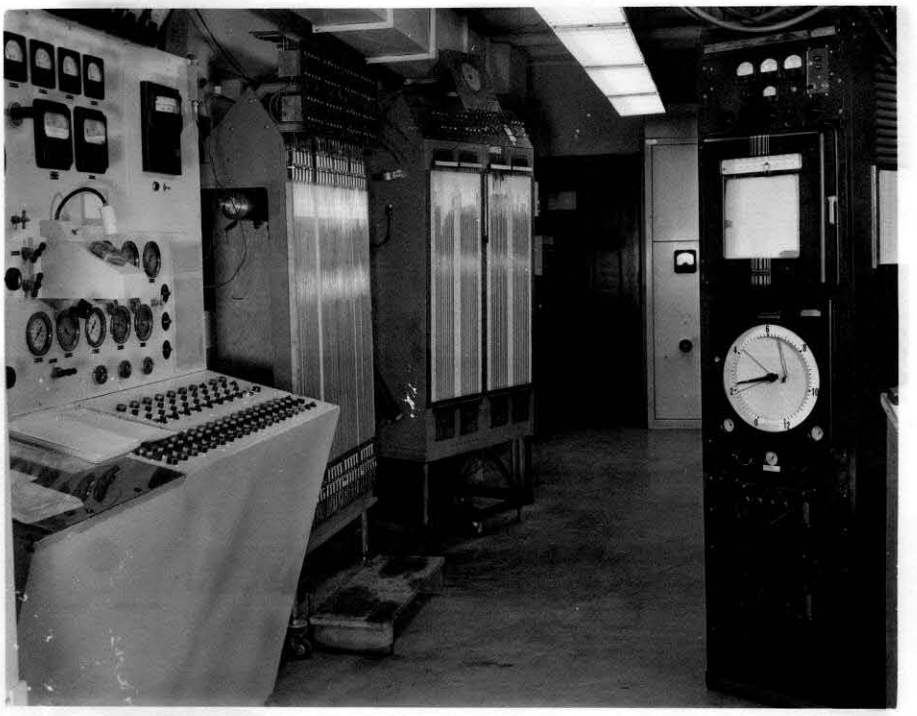

SECTION OF GALCIT HYPERSONIC WIND TUNNEL CONTROL ROOM

FIG. 2

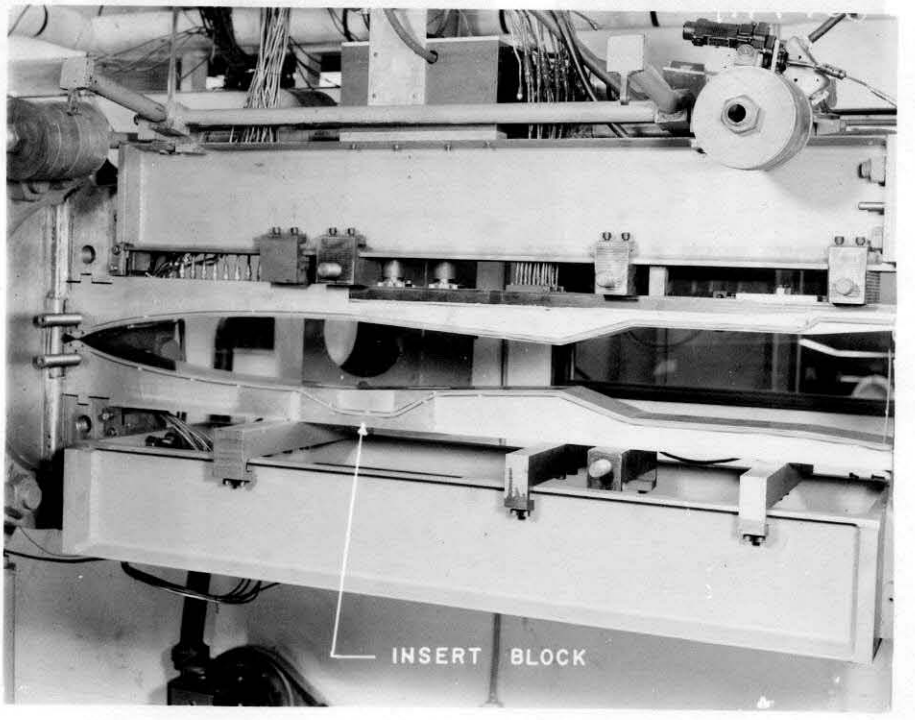

THE LEG NO. 1 REVISED TEST SECTION

FIG. 3

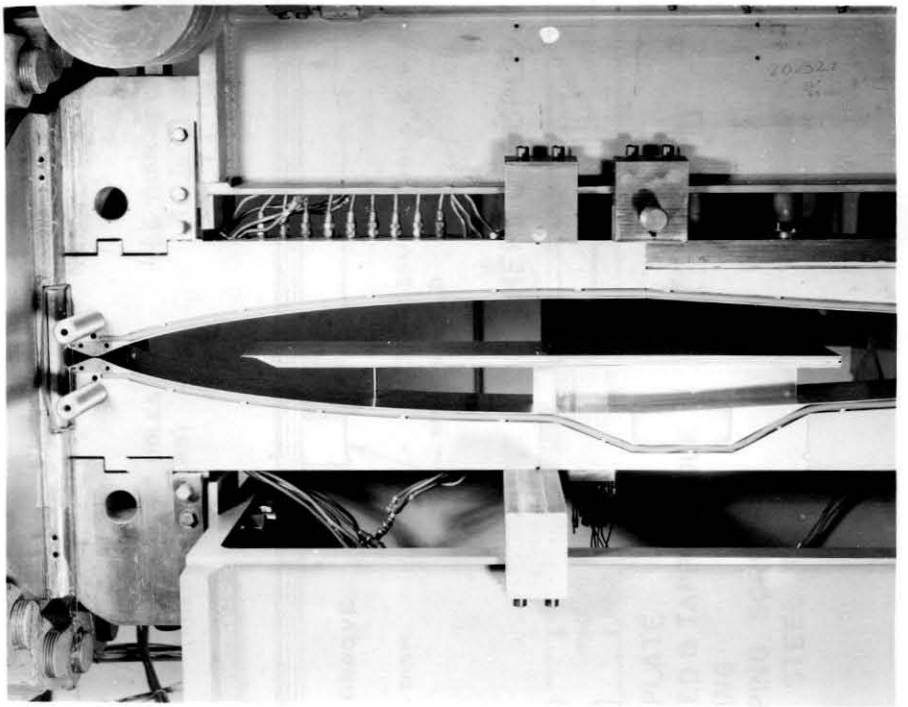

TRANSITION SURVEY FLAT PLATE IN LEG NO. 1 TEST SECTION

FIG. 4

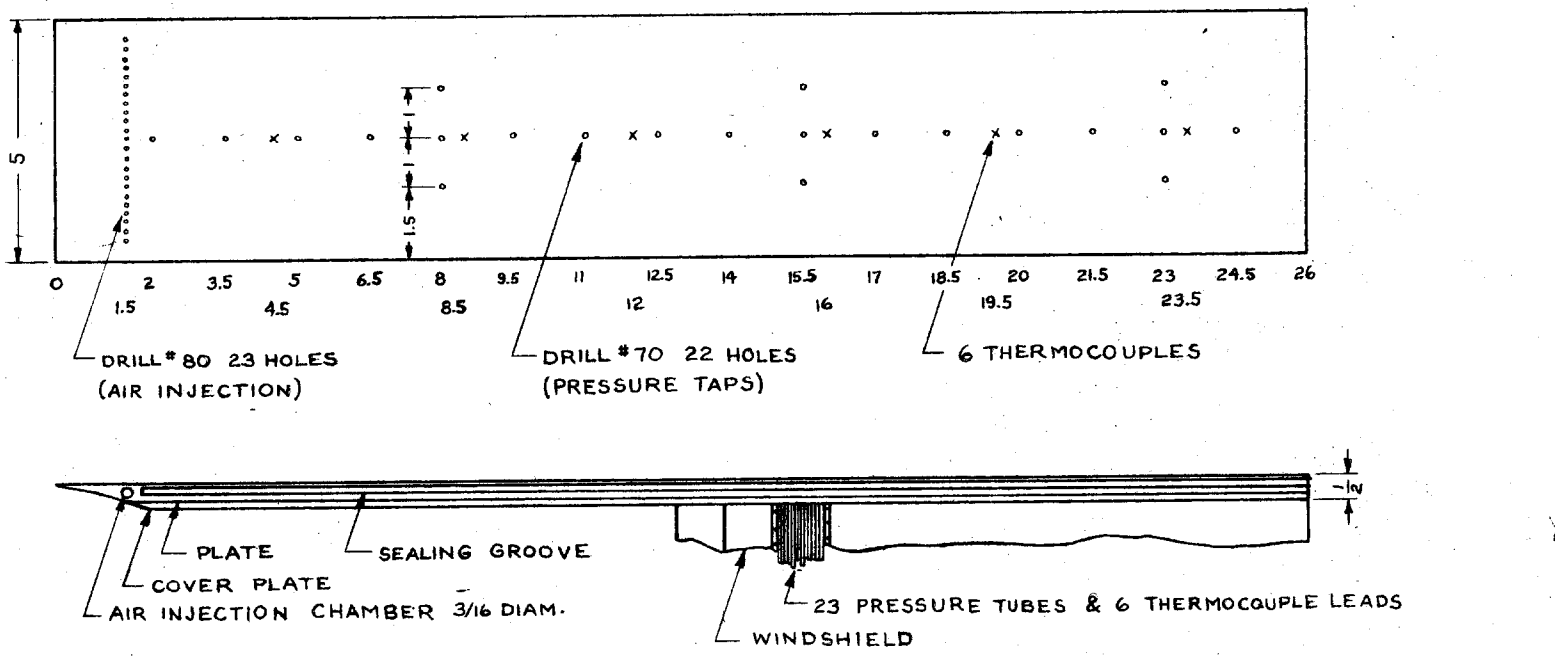

TRANSITION SURVEY FLAT PLATE

FIG. 5

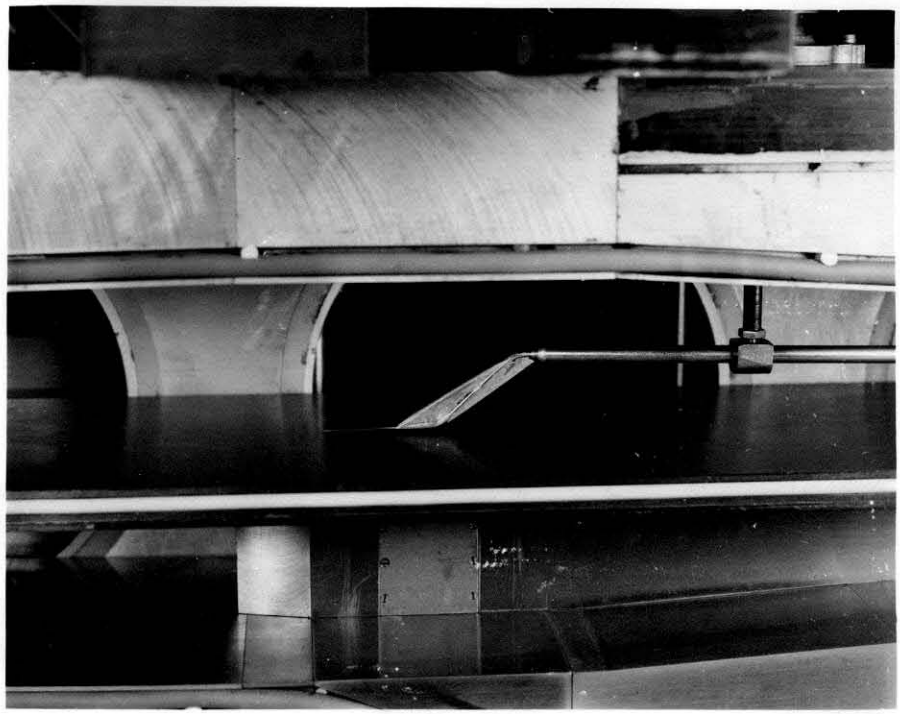

THE BOUNDARY LAYER PITOT PROBE

FIG. 6

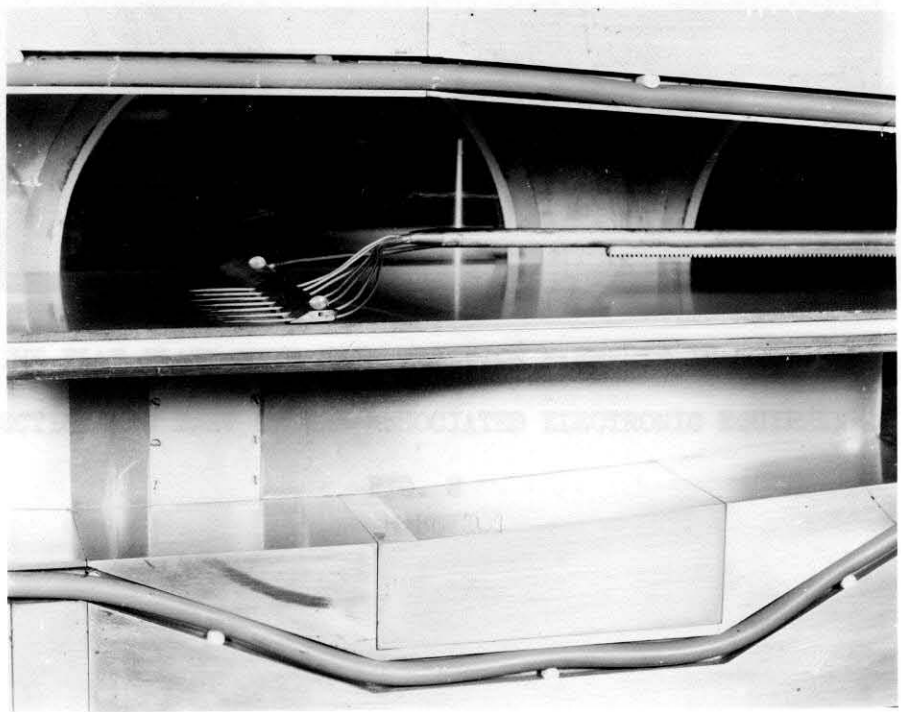

THE SEVEN-PROBE TOTAL-HEAD RAKE

FIG. 7

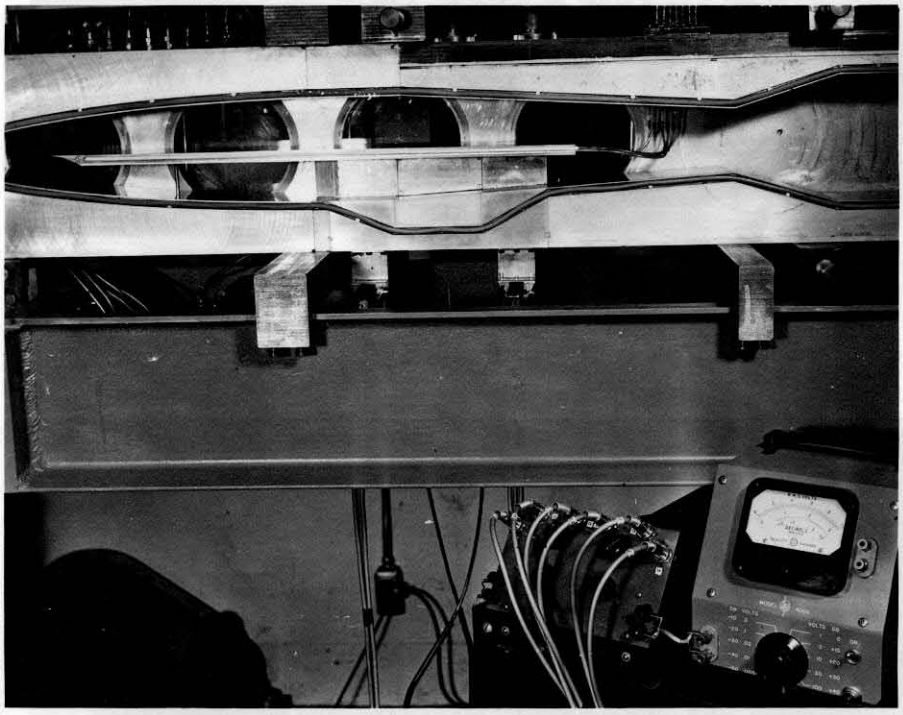

THE FLAT PLATE WITH SKIN FRICTION ELEMENTS IN THE TEST SECTION AND PART OF THE ASSOCIATED ELECTRONIC EQUIPMENT

FIG. 8

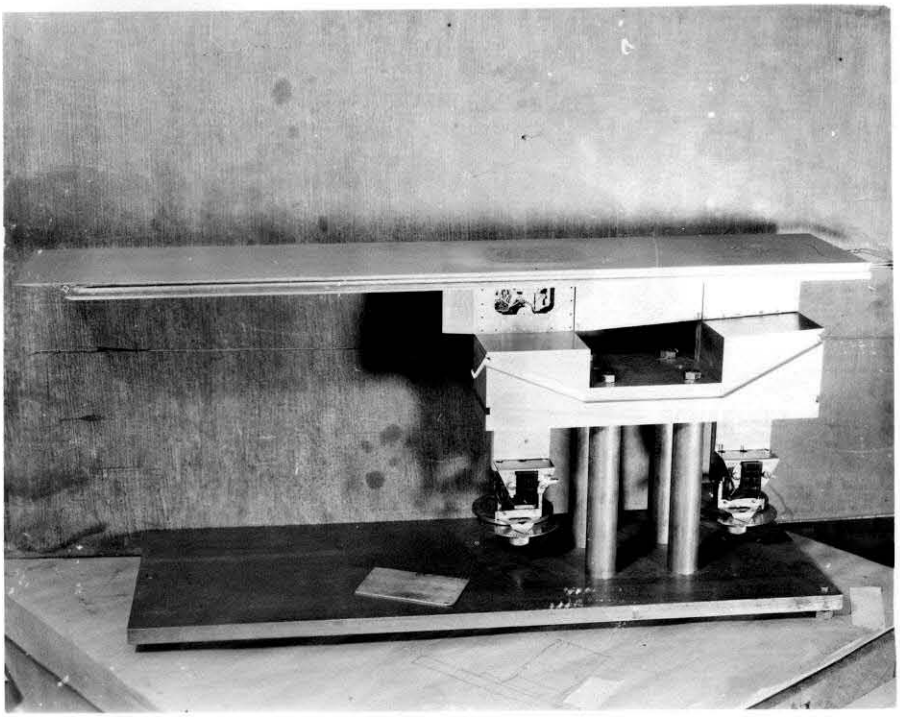

THE FLAT PLATE AND BALANCE ASSEMBLY ON A WORKING STAND

FIG. 9

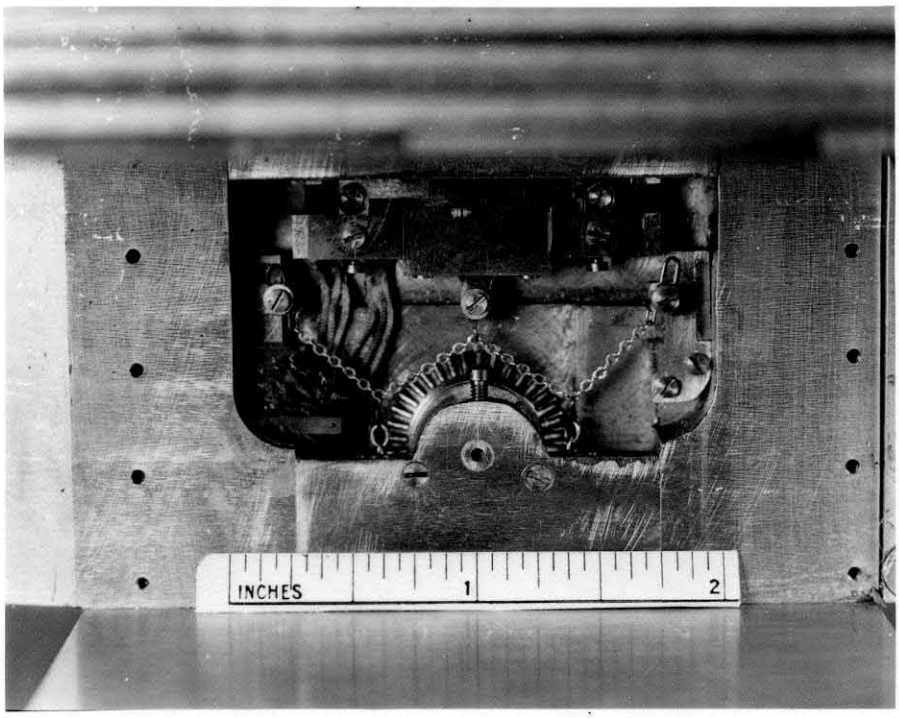

VIEW OF FRONT BALANCE AND CHAIN LINKAGE

THROUGH BALANCE CHAMBER DOOR

FIG. 10

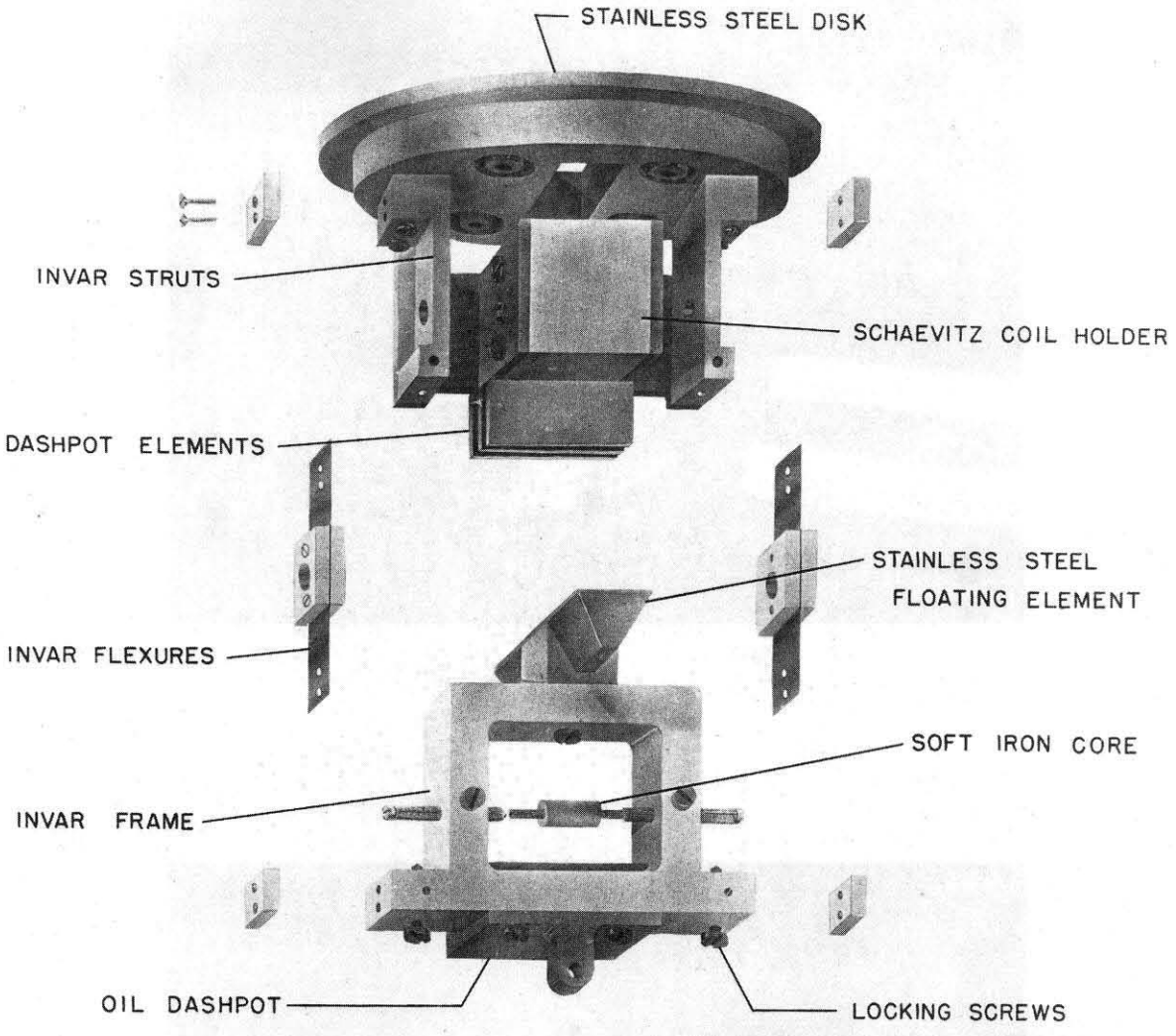

EXPLODED VIEW OF BALANCE SYSTEM

FIG. 11

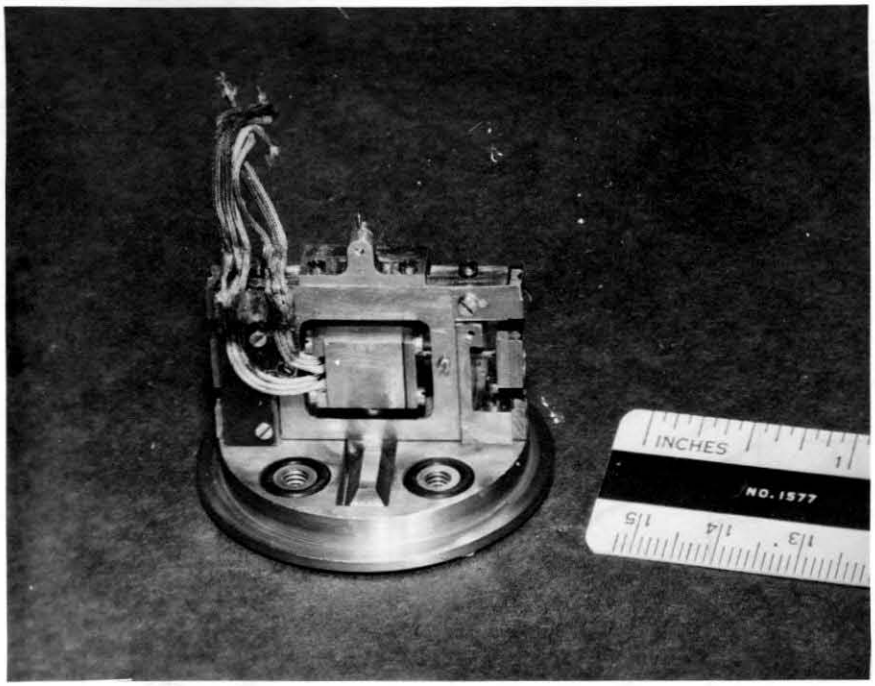

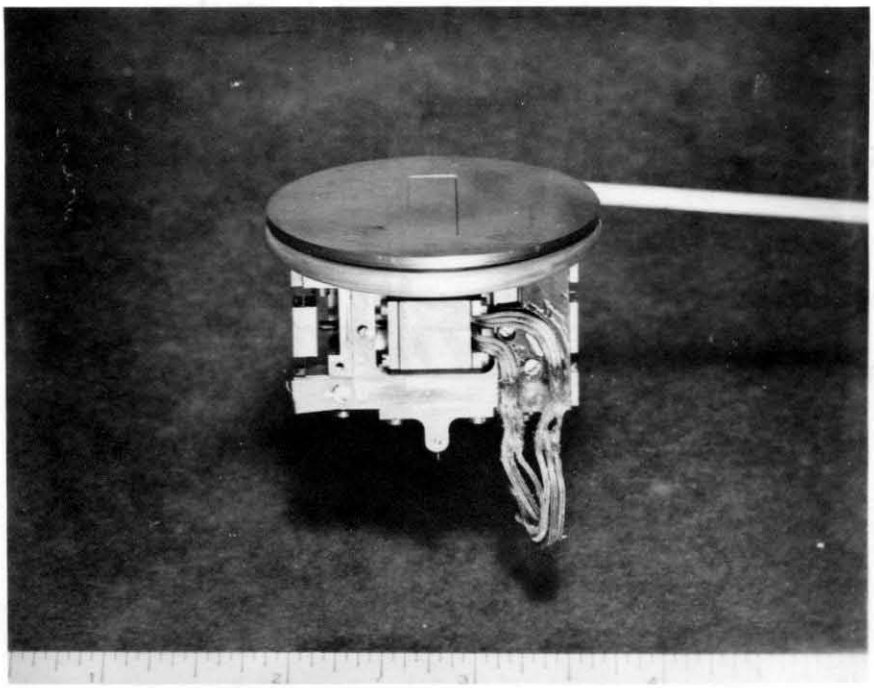

TWO VIEWS OF SKIN FRICTION BALANCE UNIT

FIG. 12

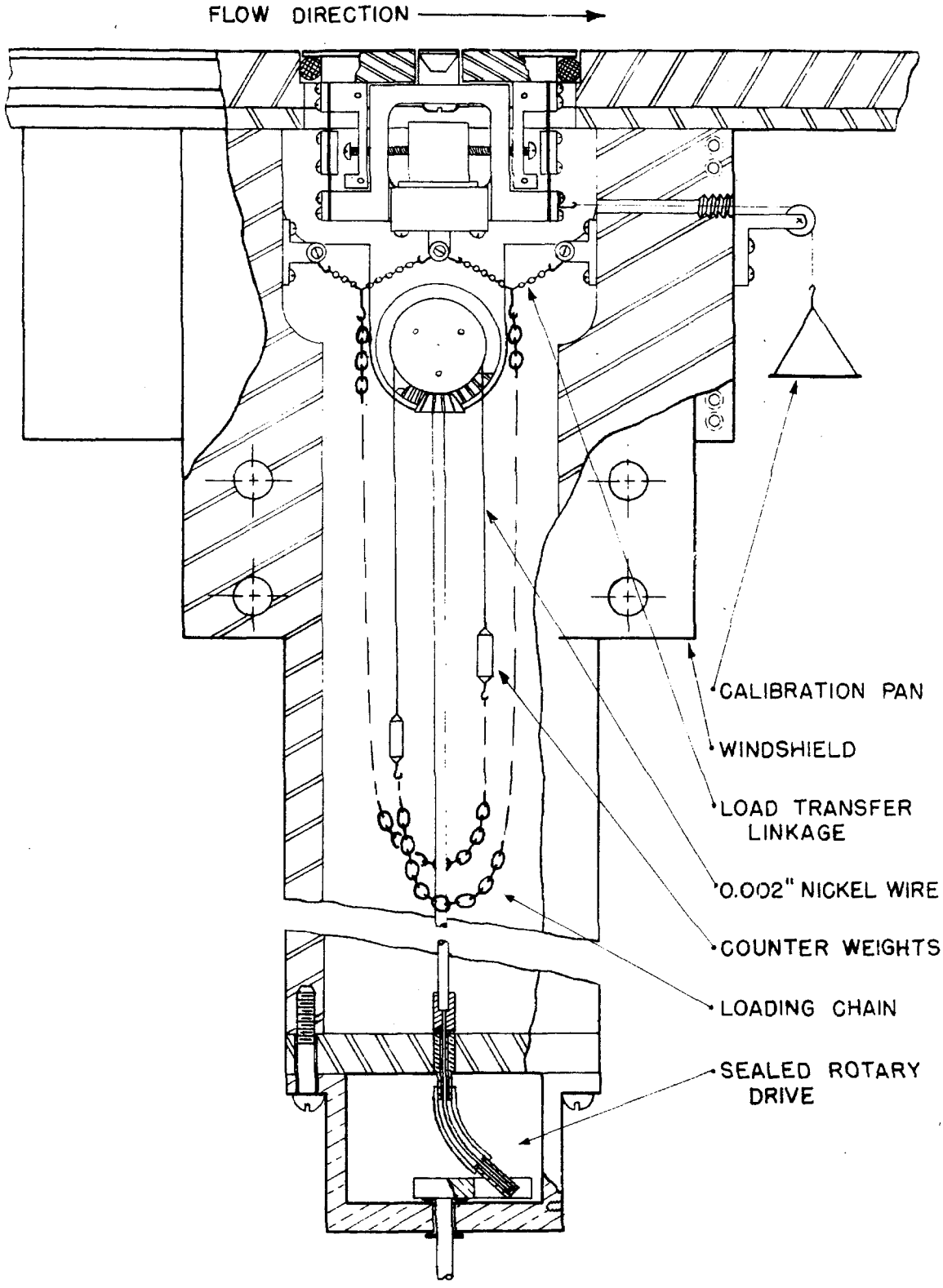

BALANCE ASSEMBLY

FIG. 13

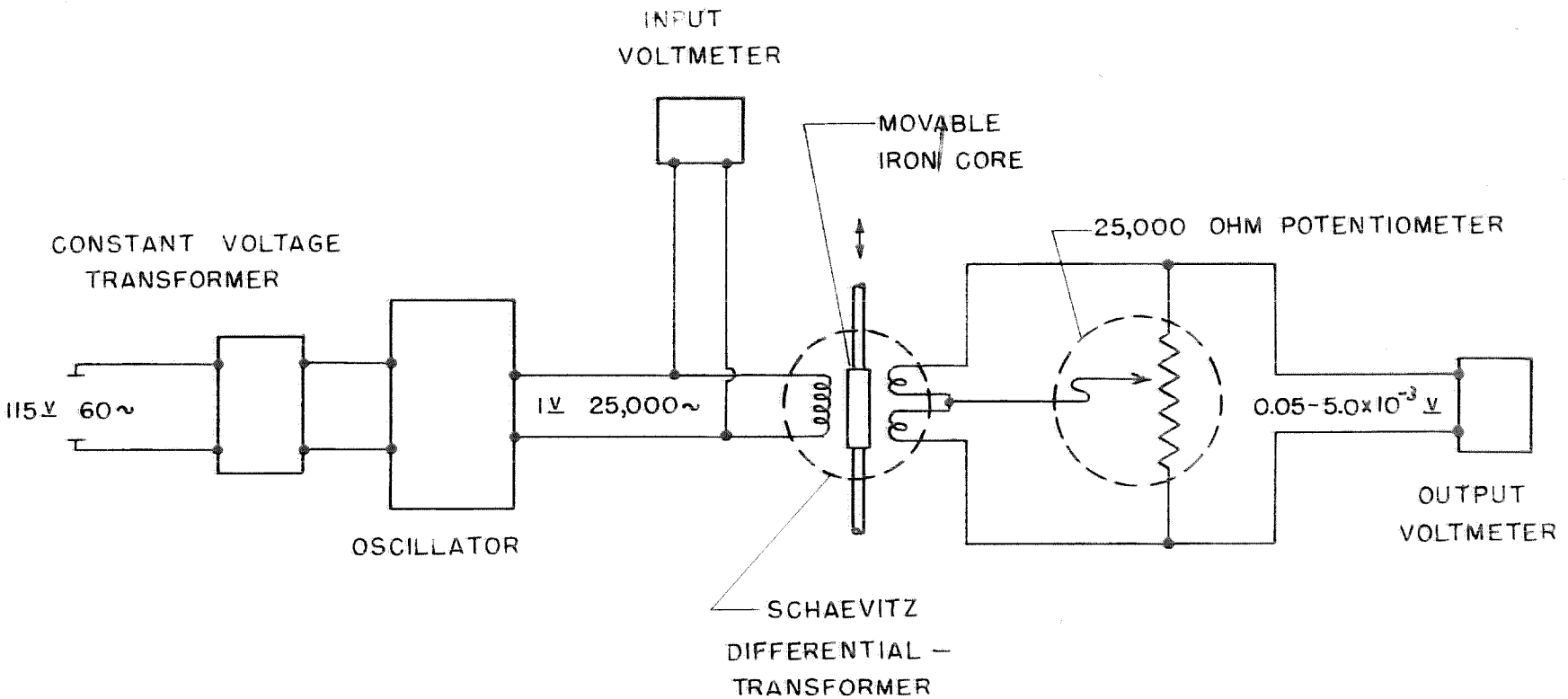

POSITION SENSING CIRCUIT

FIG. 14

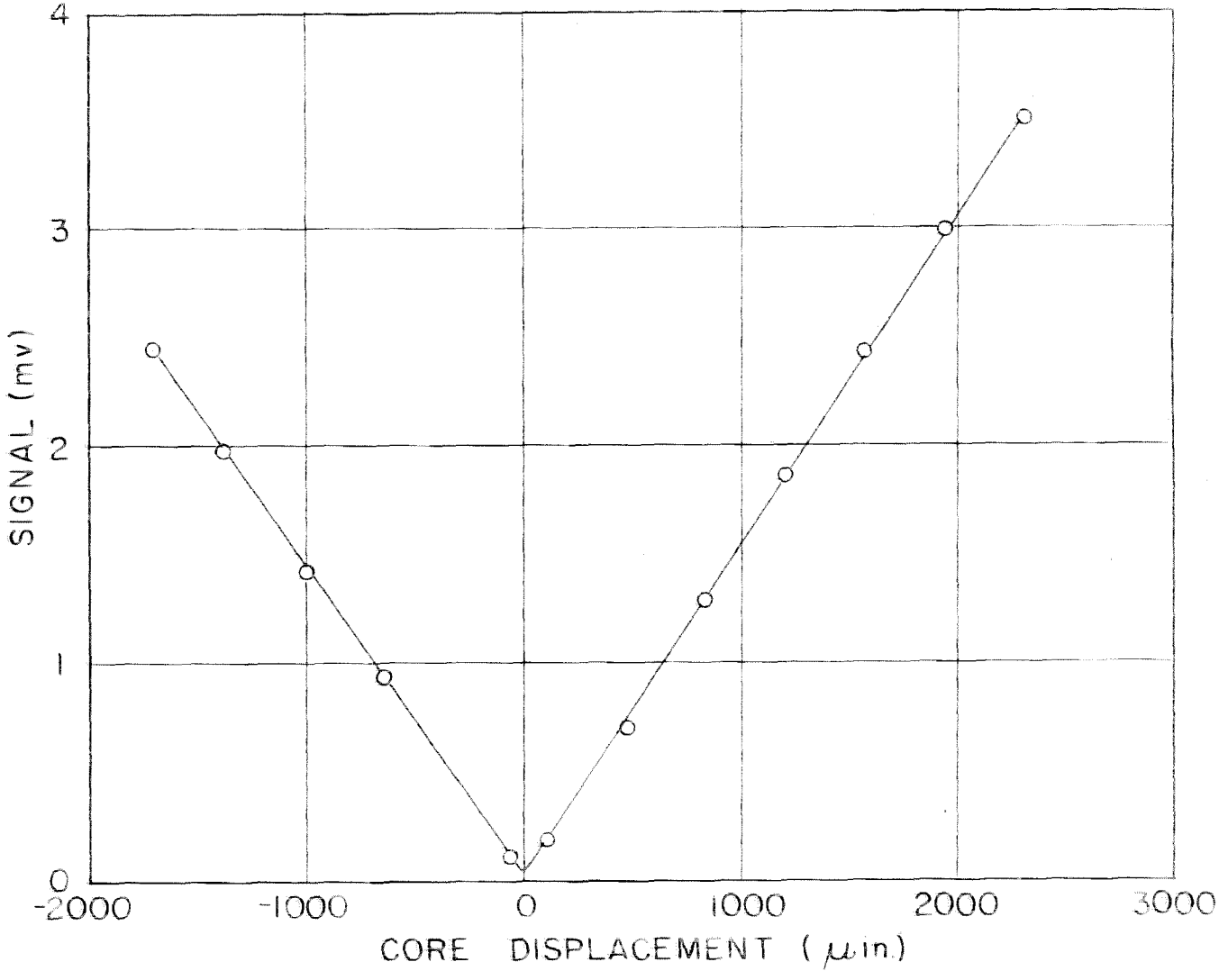

TYPICAL OUTPUT SIGNAL OF SCHAEVITZ L.V.D. TRANSFORMER

FIG. 15

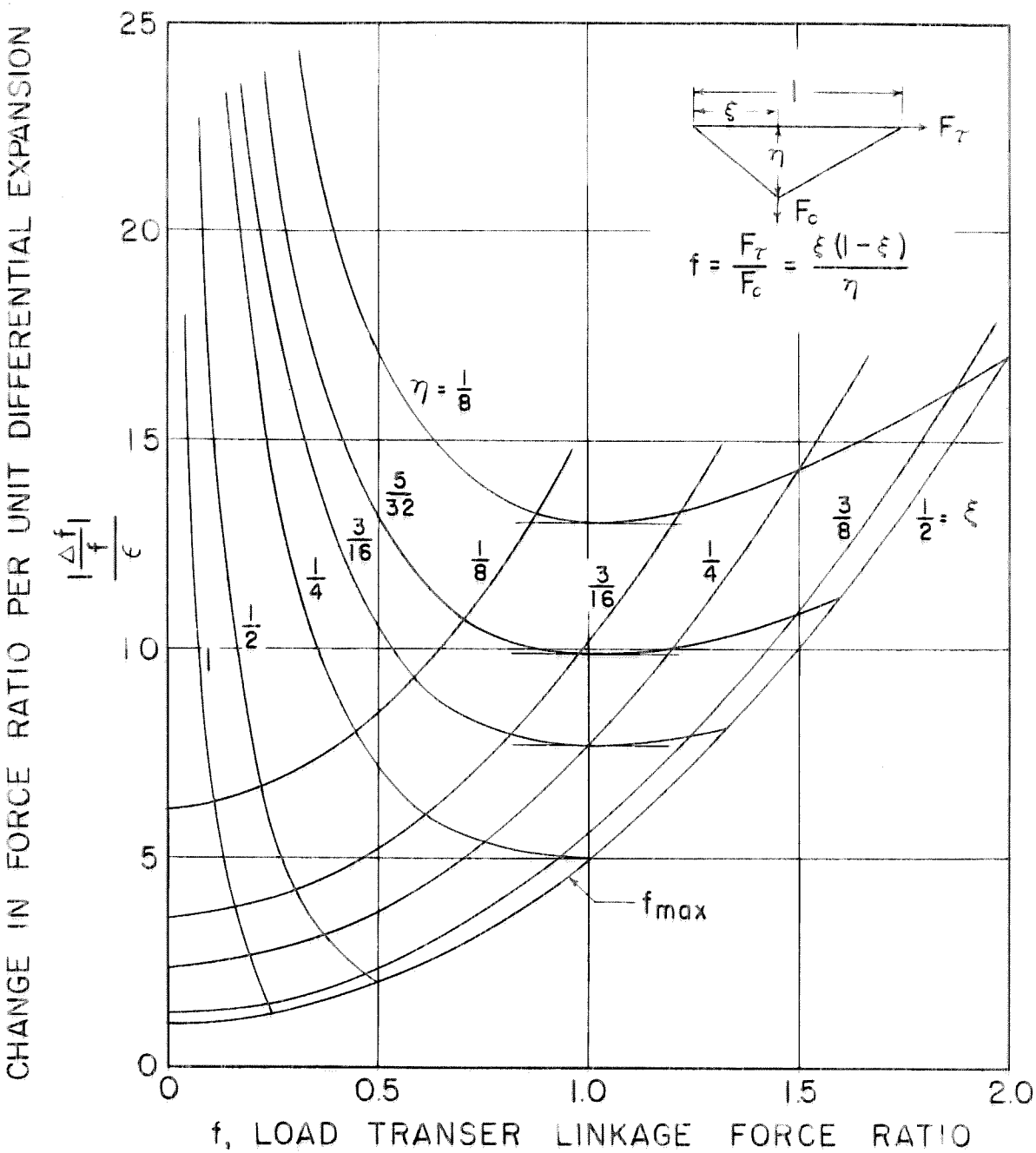

EFFECT OF TEMPERATURE ON FORCE RATIO

FIG. 16

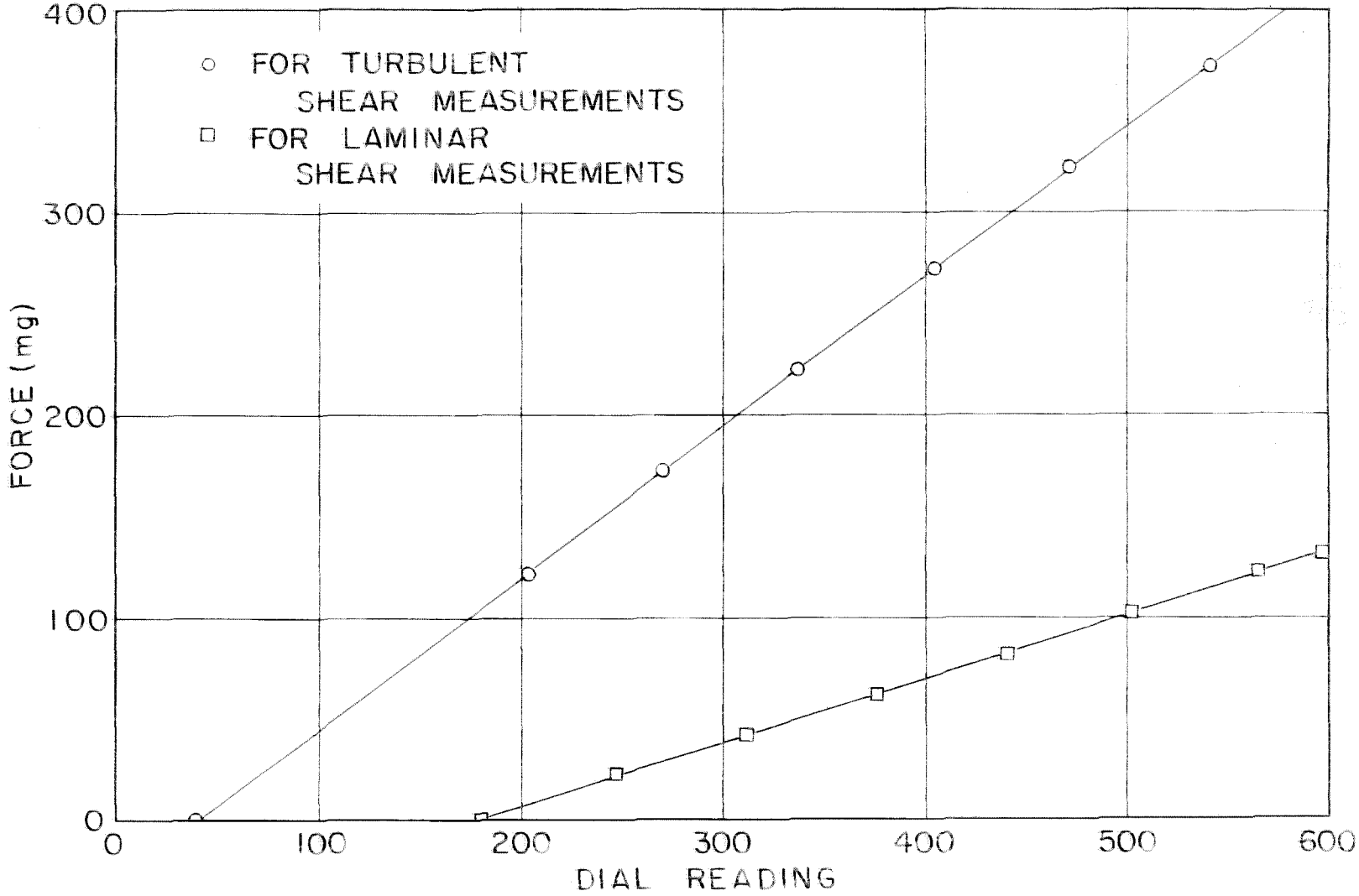

BALANCE FORCE CALIBRATION CURVES

FIG. 17

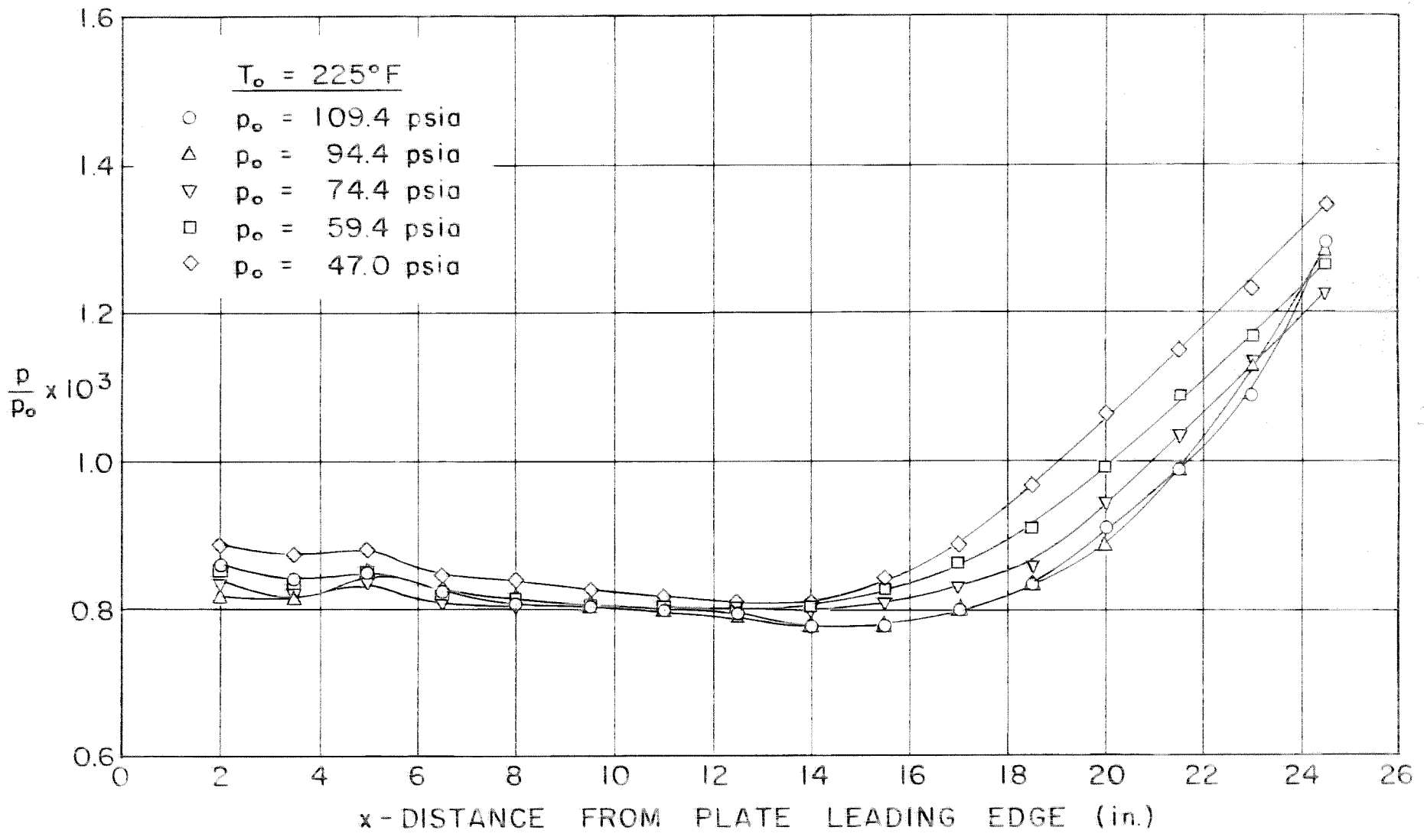

FLAT PLATE SURFACE PRESSURES

FIG. 18

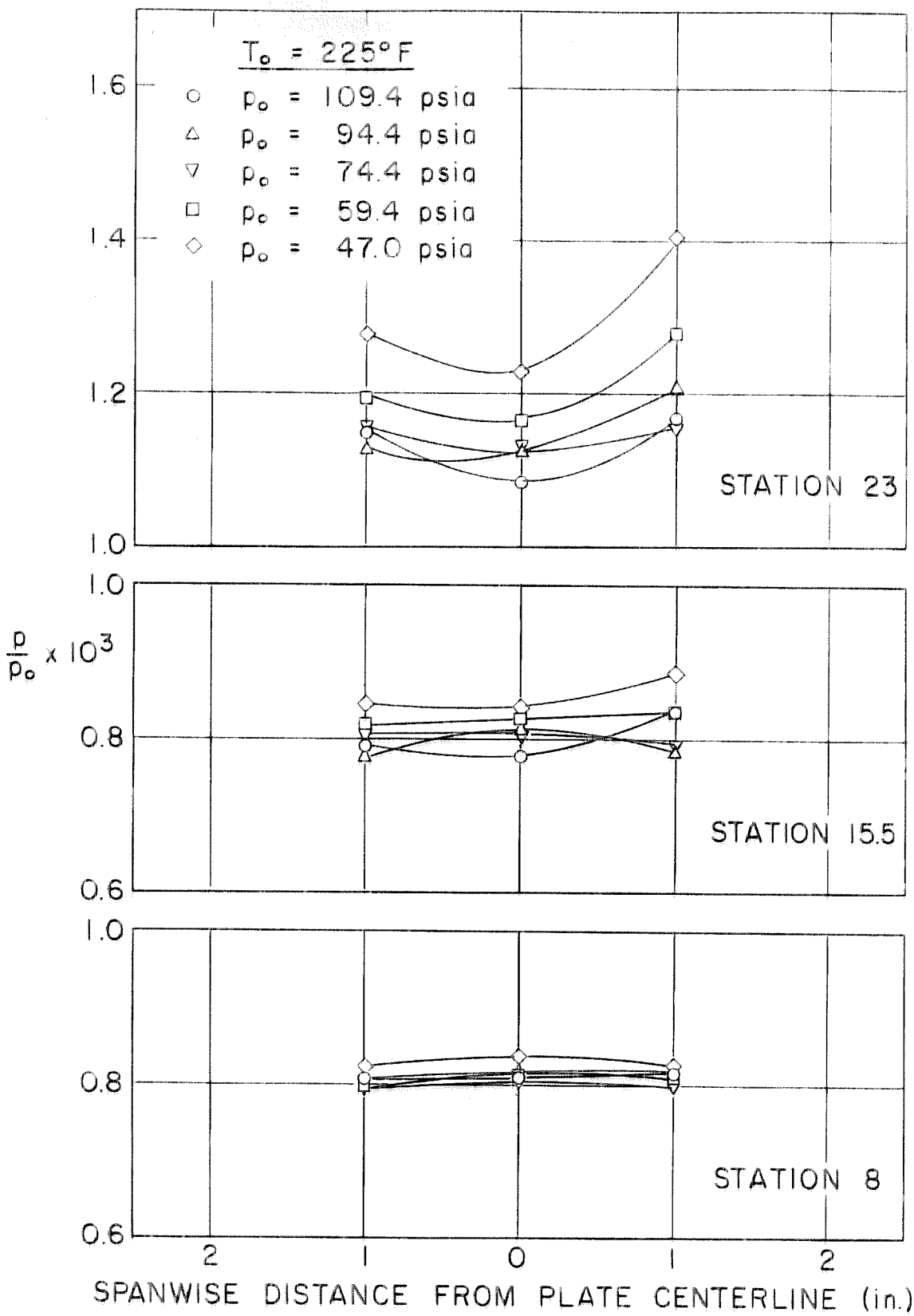

FLAT PLATE SURFACE PRESSURES

FIG. 19

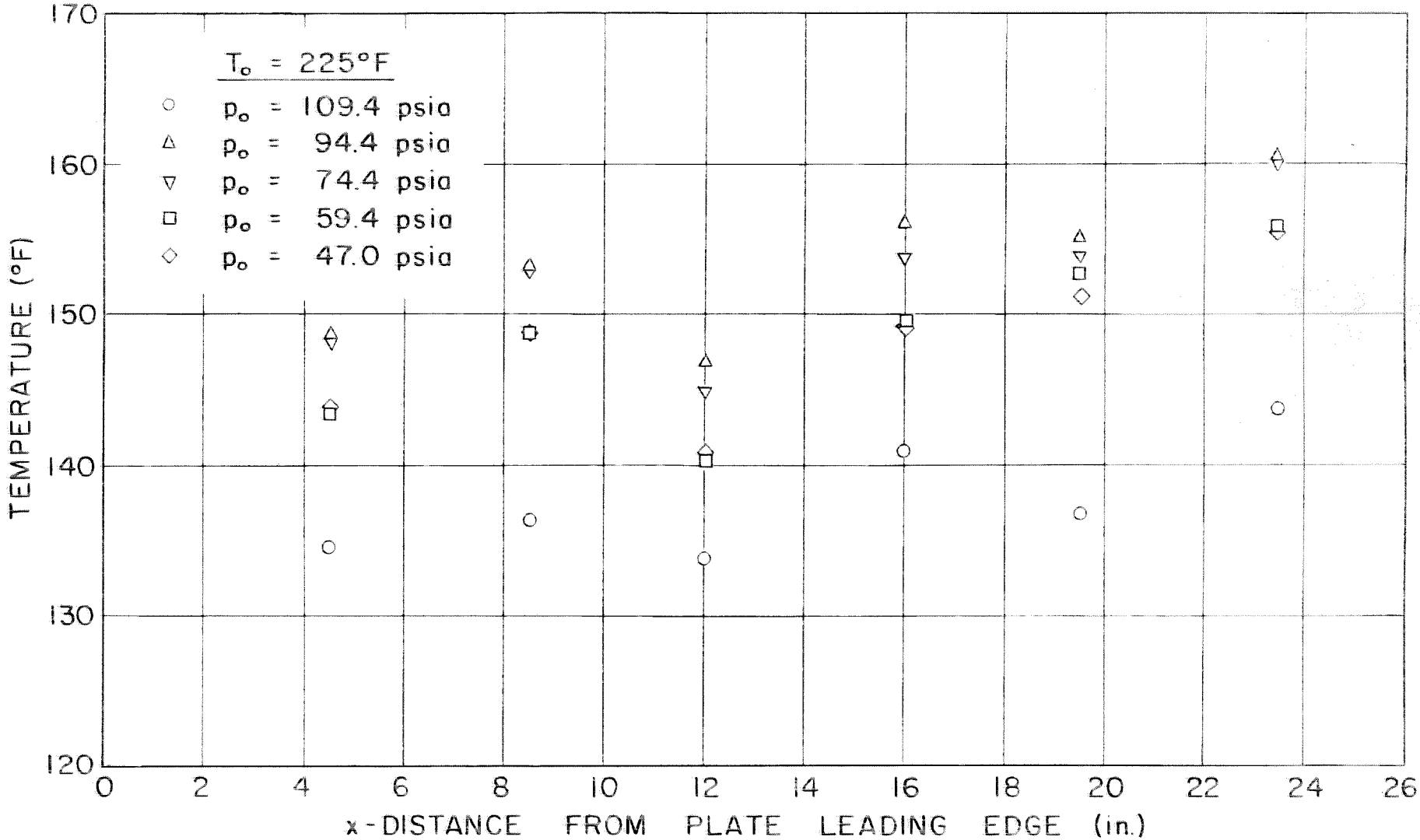

FLAT PLATE SURFACE TEMPERATURES

FIG. 20

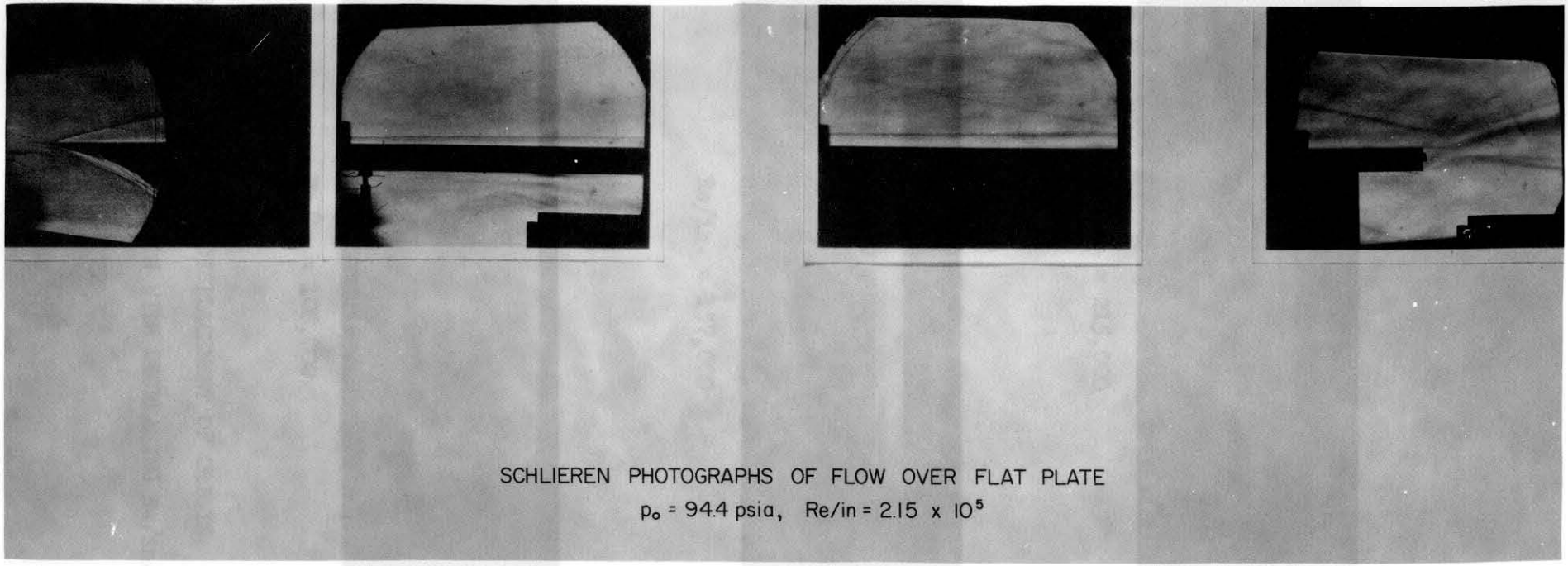

SCHLIEREN PHOTOGRAPHS OF FLOW OVER FLAT PLATE

p_o = 94.4 psia, Re/in = 2.15 x 10^5

FIG. 21

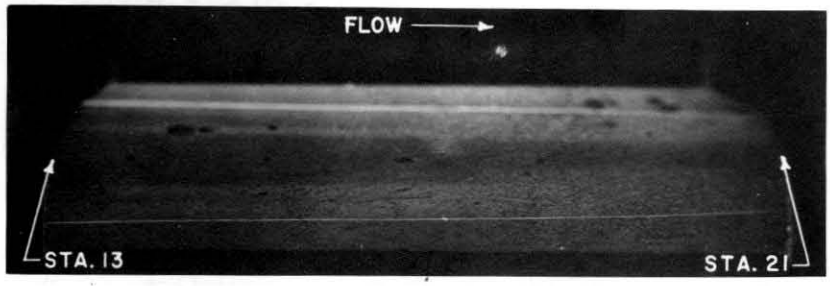

Re/in. = 215,000

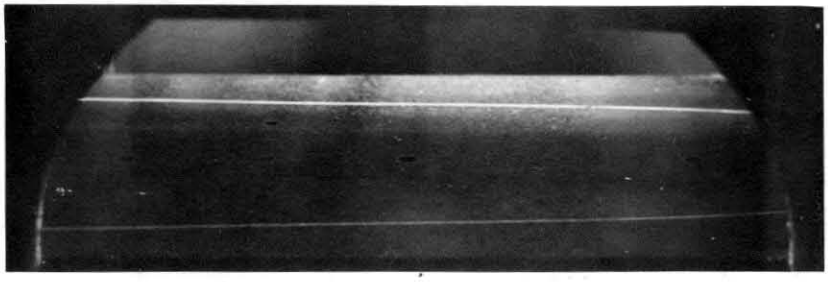

Re/in. = 157,000

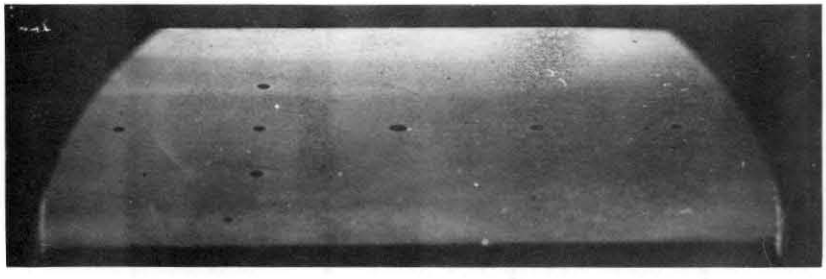

Re/in = 108,000

PROGRESSIVE DOWNSTREAM DISPLACEMENT OF ORIGIN OF TRANSVERSE CONTAMINATION WITH DECREASING Re/in.

FIG. 22

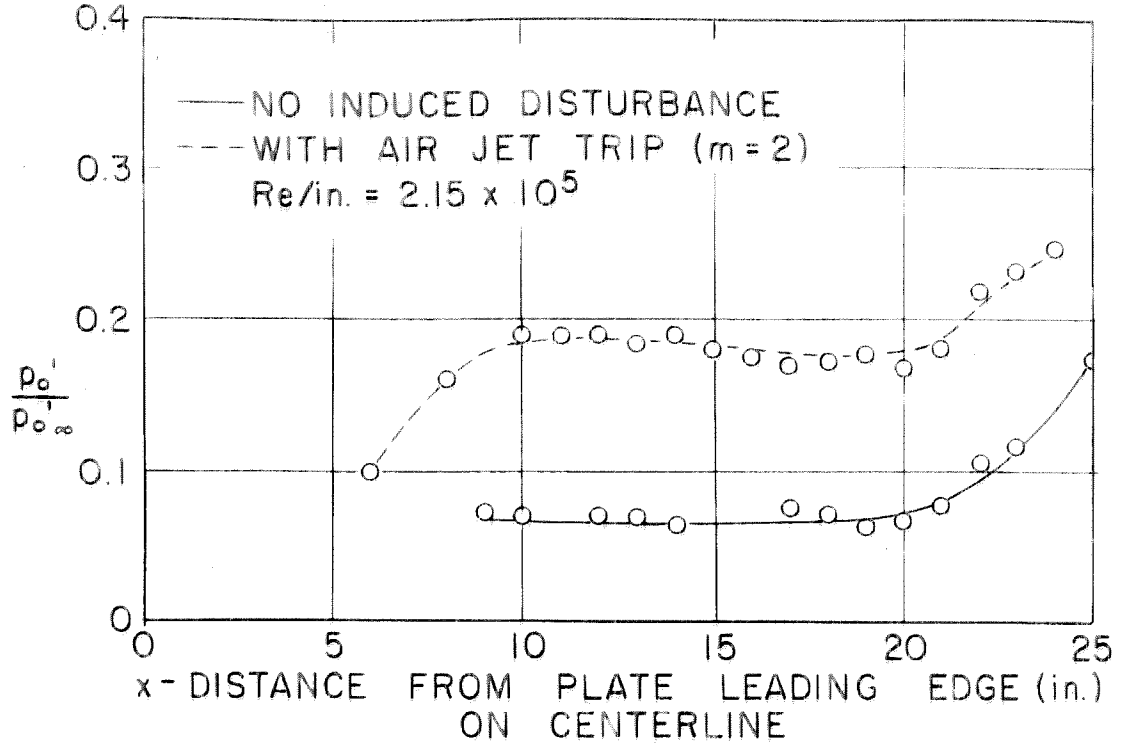

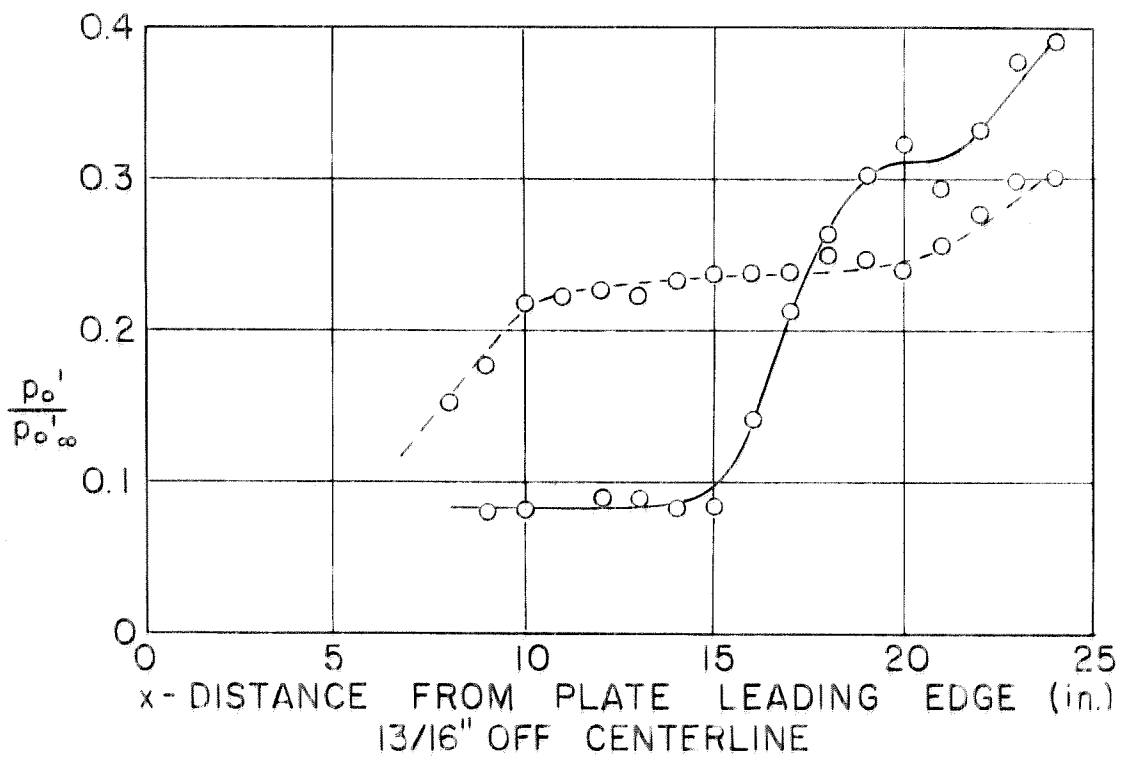

TYPICAL AXIAL IMPACT PRESSURE DISTRIBUTION
1/16" ABOVE PLATE SURFACE

FIG. 23

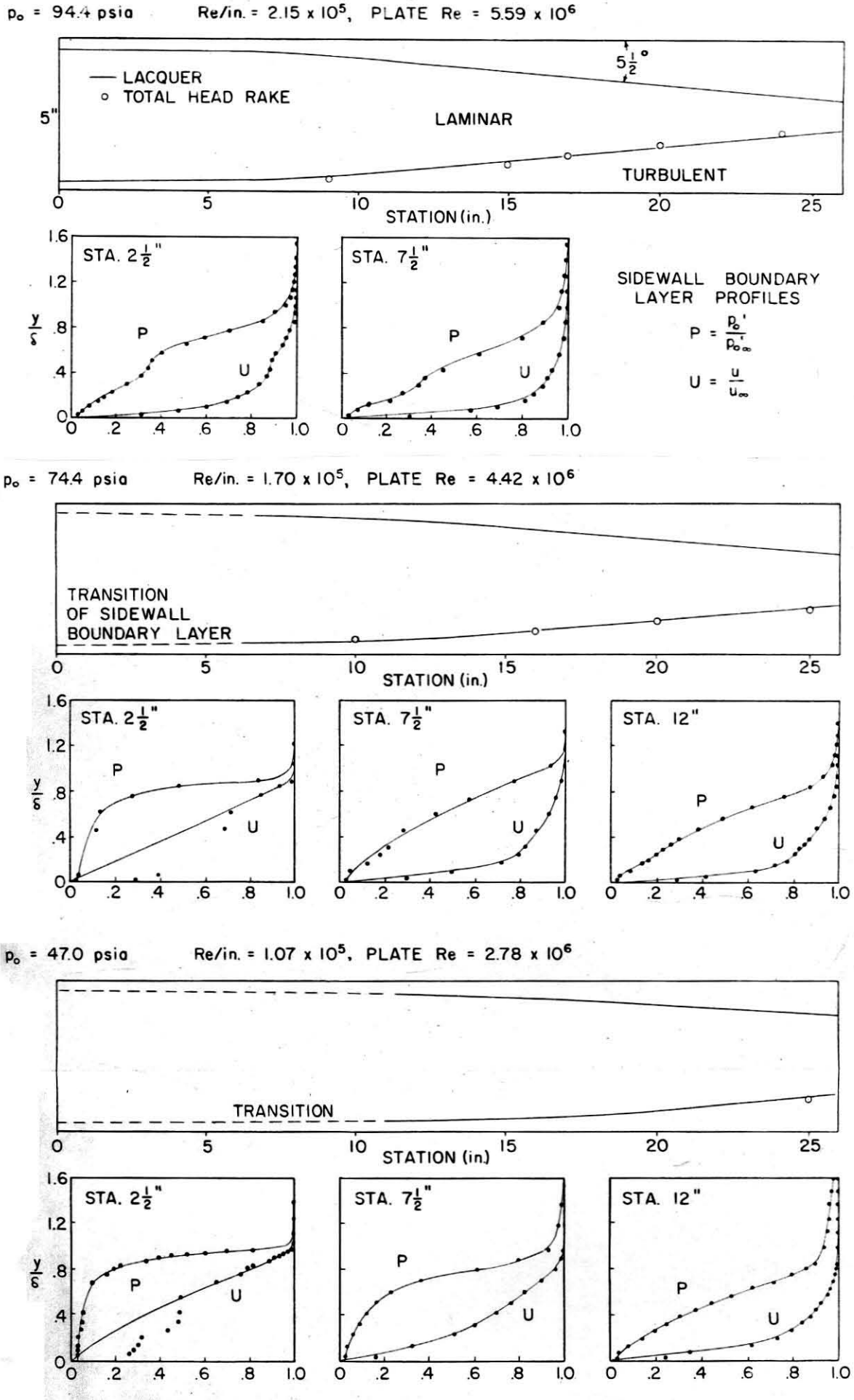

TRANSVERSE CONTAMINATION AND SIDEWALL BOUNDARY LAYER ON FLAT PLATE AT DIFFERENT REYNOLDS NUMBERS

FIG. 24

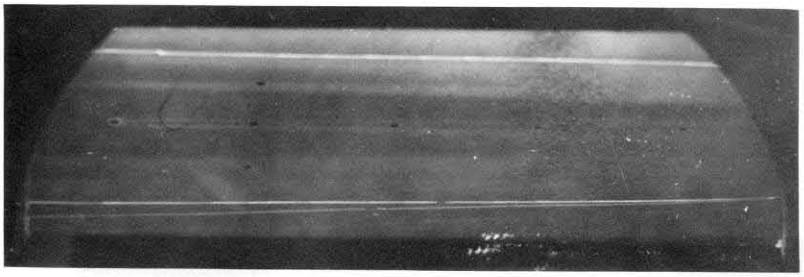

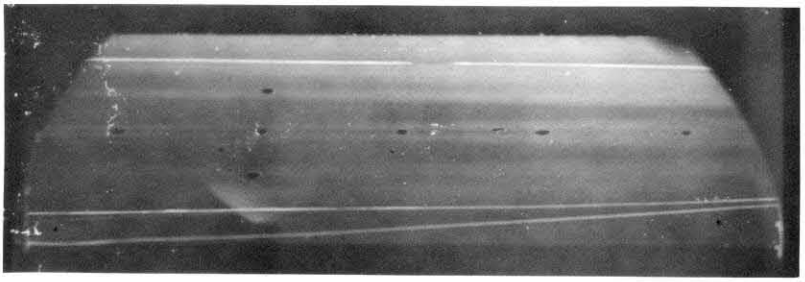

WAKE OF AIR JET AND SUBSEQUENT SPREAD OF CONTAMINATION

FIG. 25

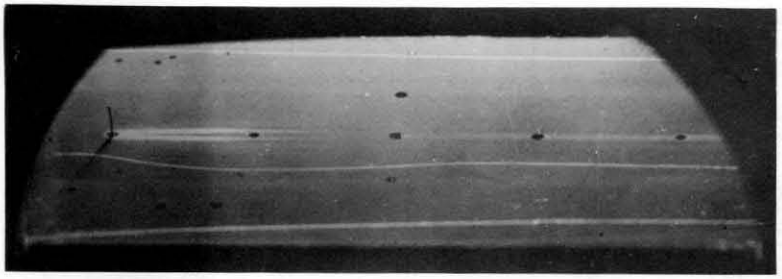

WAKE OF ROD WITH NO SPREAD OF CONTAMINATION

FIG. 26

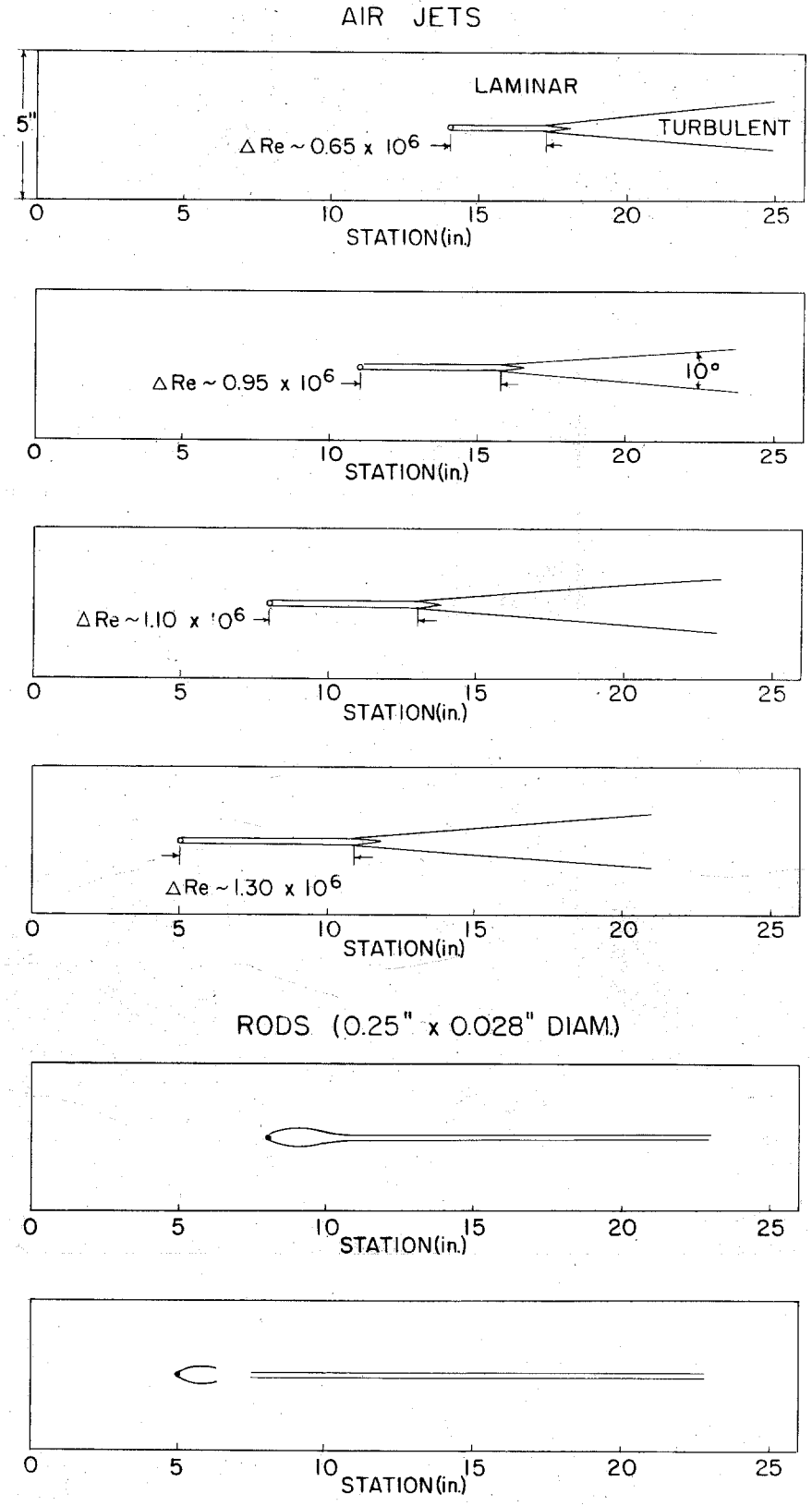

CONTAMINATION ON FLAT PLATE DUE TO LOCAL DISTURBANCES
p_o = 94.4 psia, Re/in. = 2.15 x 10^5, PLATE Re = 5.59 x 10^6

FIG. 27

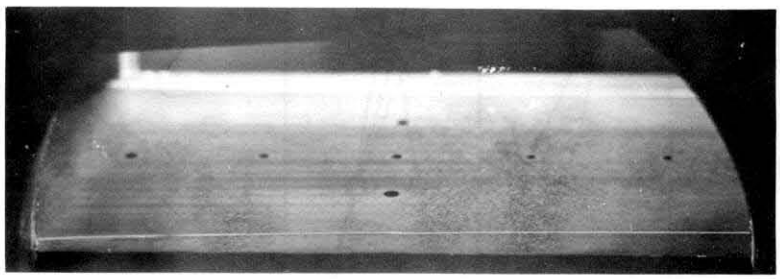

$Re = 2 \times 10^6$

WAKE OF AIR JETS AND INDUCED TRANSITION (m = 2)

FIG. 28

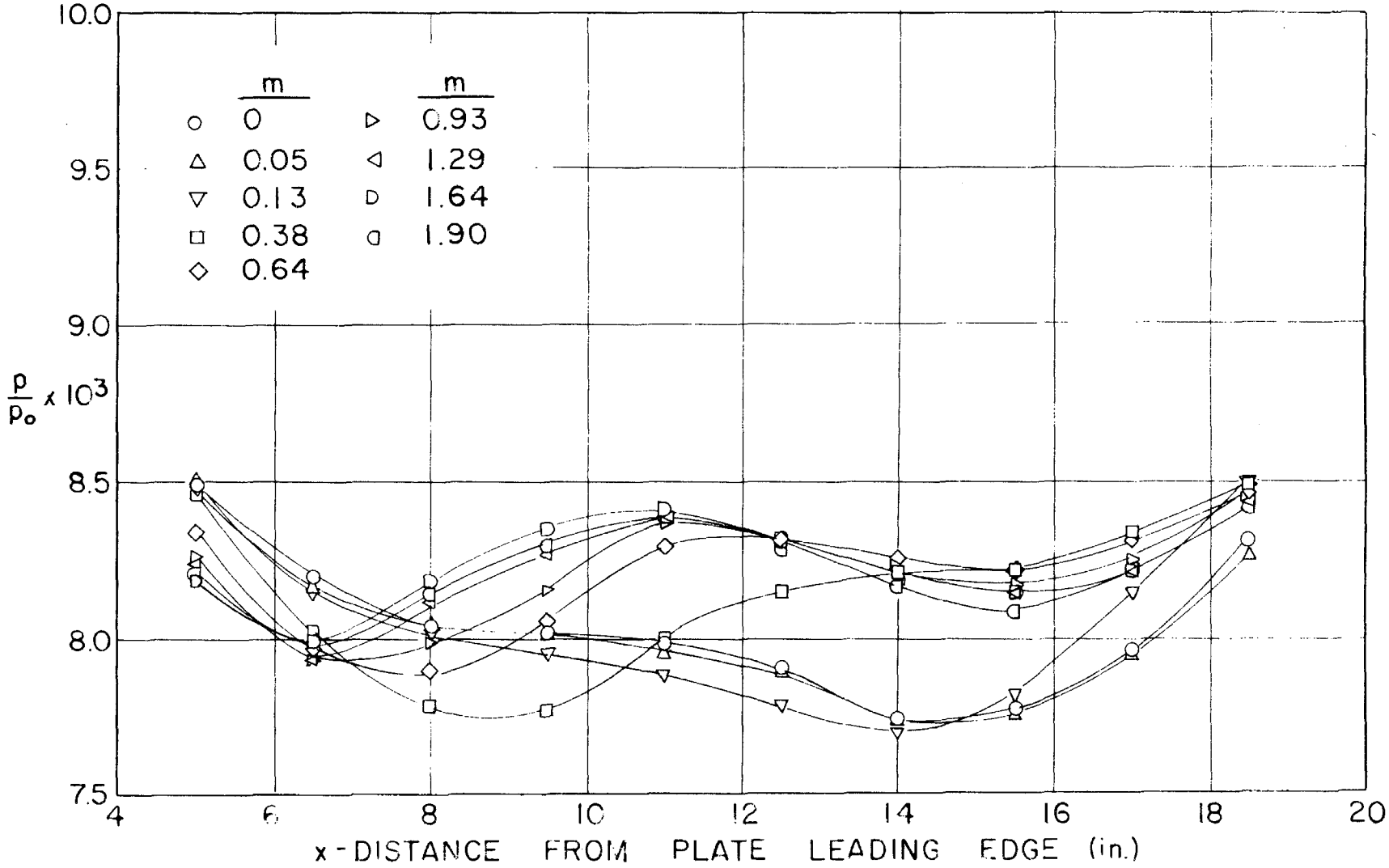

FLAT PLATE SURFACE PRESSURES WITH VARIABLE AIR INJECTION

p_o = 109.4 psia, T_o = 225°F, Re/in. = 2.50 x 10^5

FIG. 29

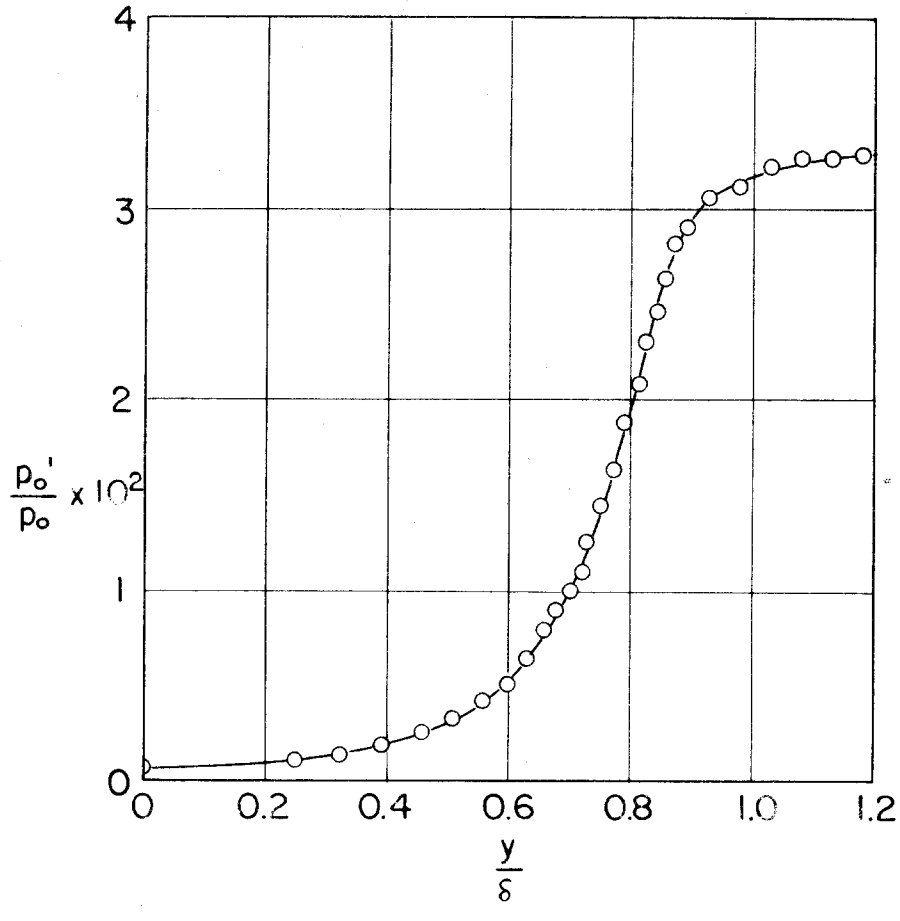

LAMINAR

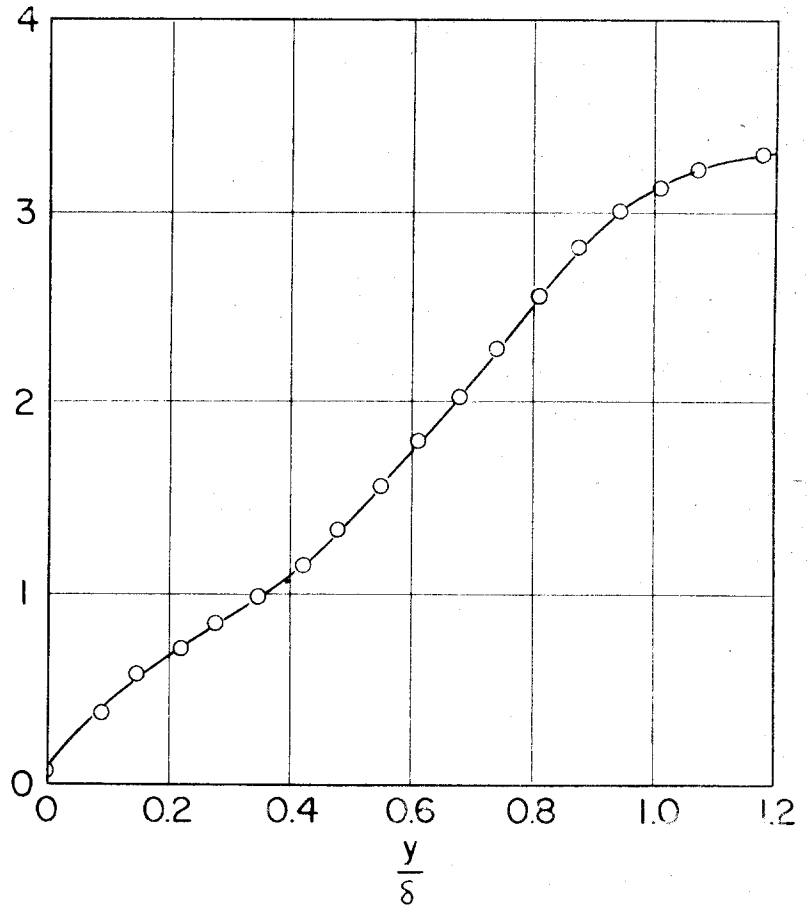

TURBULENT

TYPICAL IMPACT PRESSURE DISTRIBUTION IN THE BOUNDARY LAYER AT M = 5.8

FIG. 30

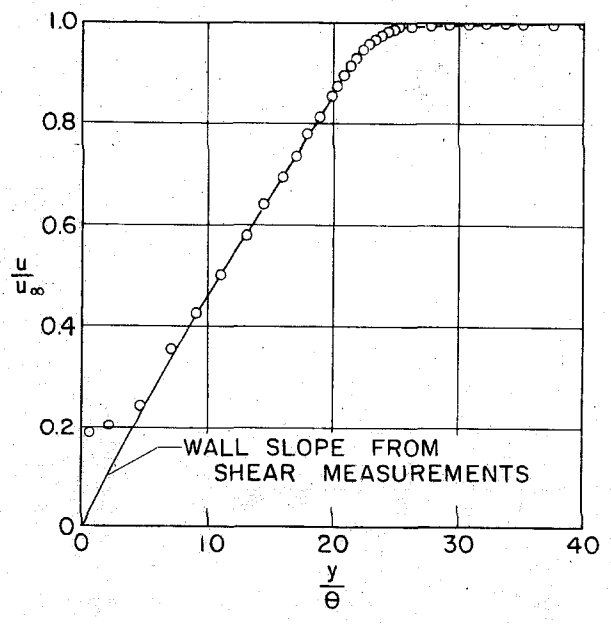

VELOCITY

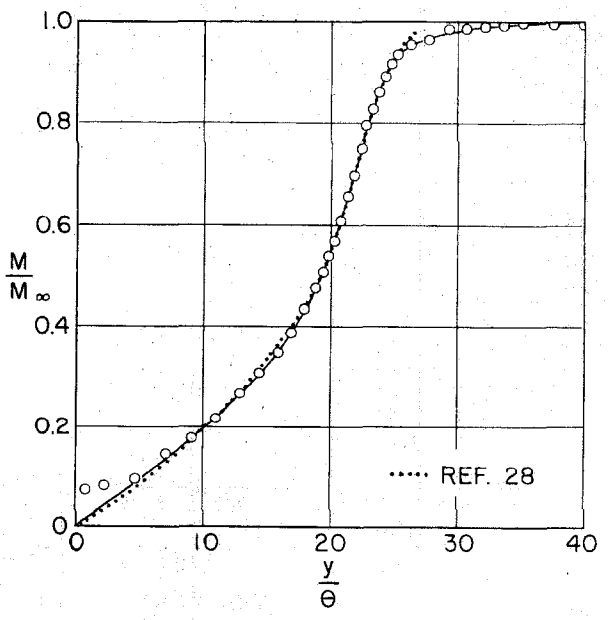

MACH NUMBER

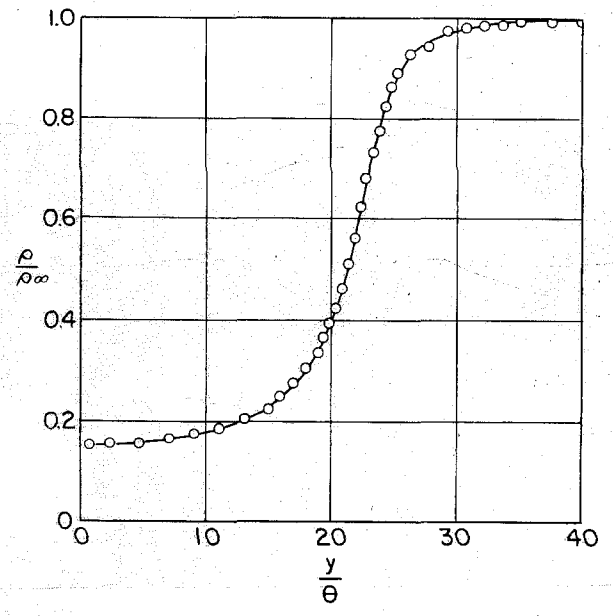

DENSITY

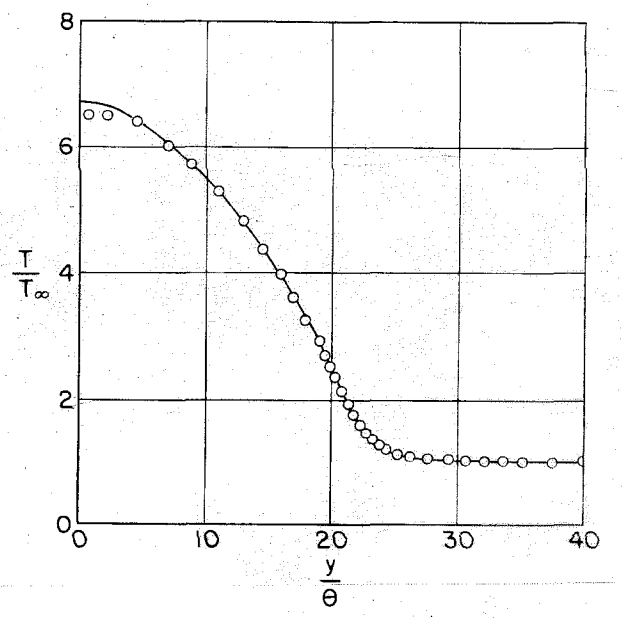

TEMPERATURE

δ = 0.290 in.
δ^* = 0.209 in.
θ = 0.0102 in.
R_θ = 2190
p_o = 94.4 psia, T_o = 225°F

DISTRIBUTION OF FLOW VARIABLES IN A TYPICAL LAMINAR BOUNDARY LAYER AT M=5.8

FIG. 31

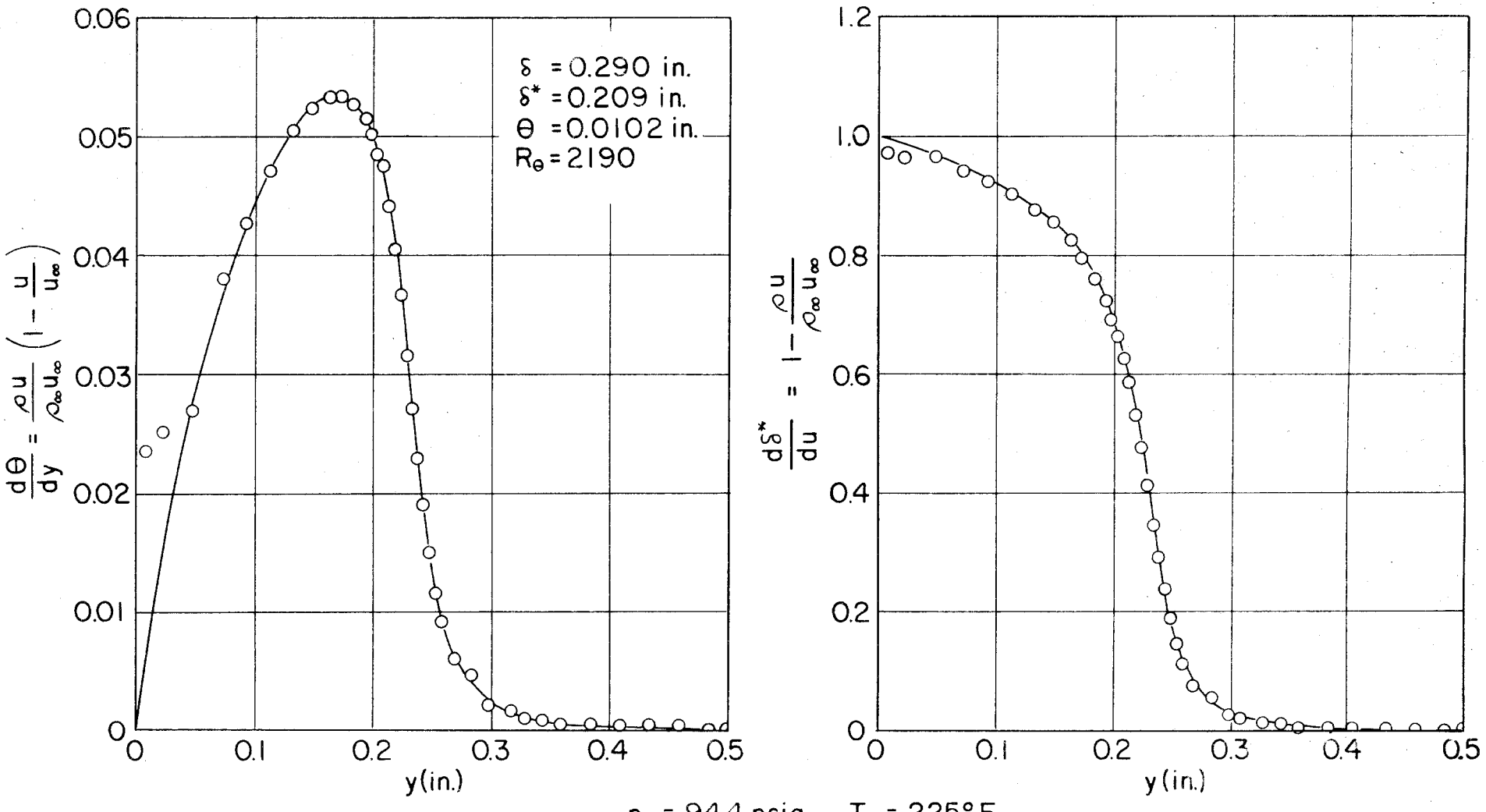

p_o = 94.4 psia, T_o = 225° F

TYPICAL MOMENTUM AND MASS DEFECT DISTRIBUTION IN A LAMINAR BOUNDARY LAYER AT M=5.8

FIG. 32

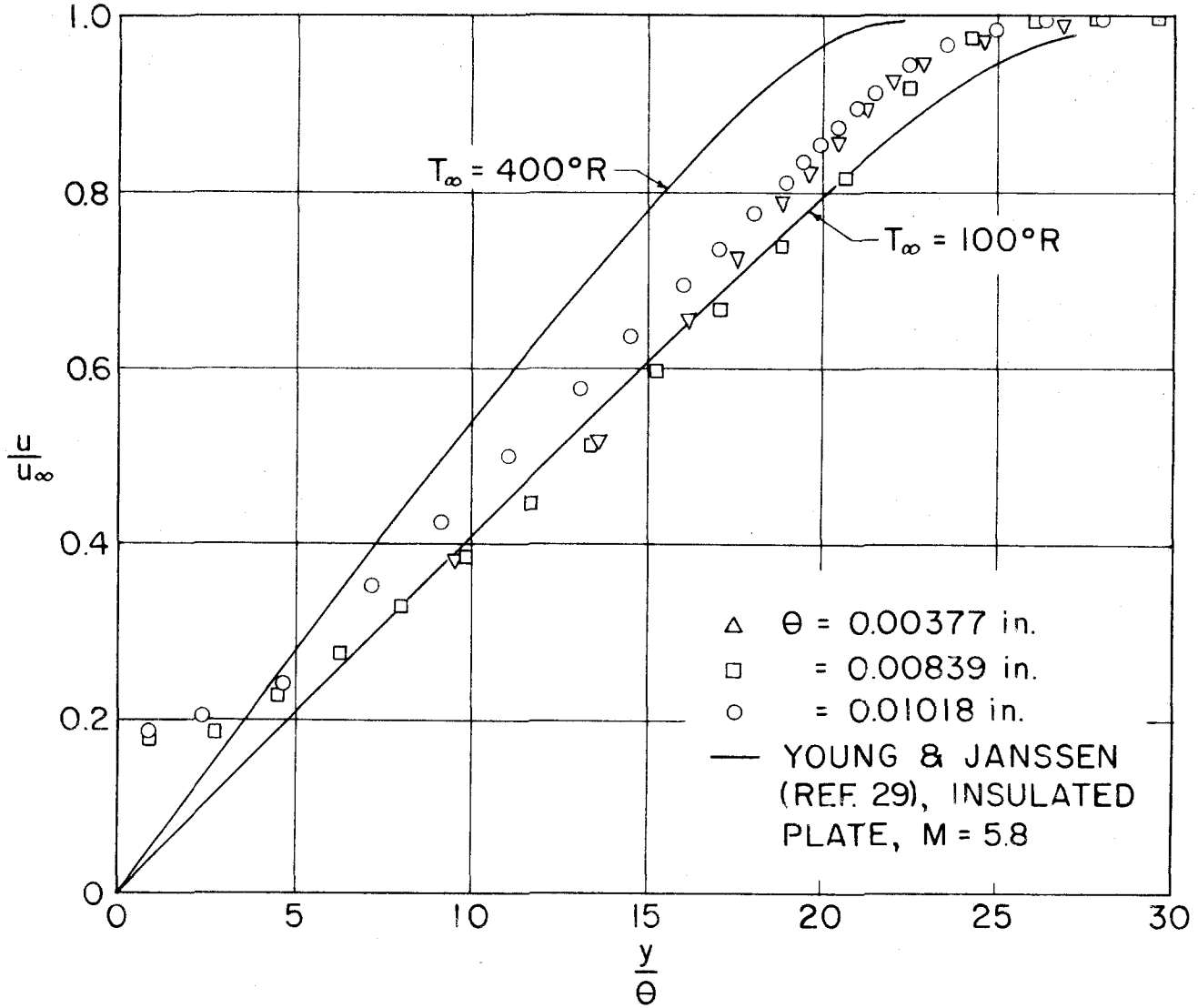

COMPARISON OF LAMINAR BOUNDARY LAYER VELOCITY PROFILES AT M = 5.8 WITH THEORY

FIG. 33

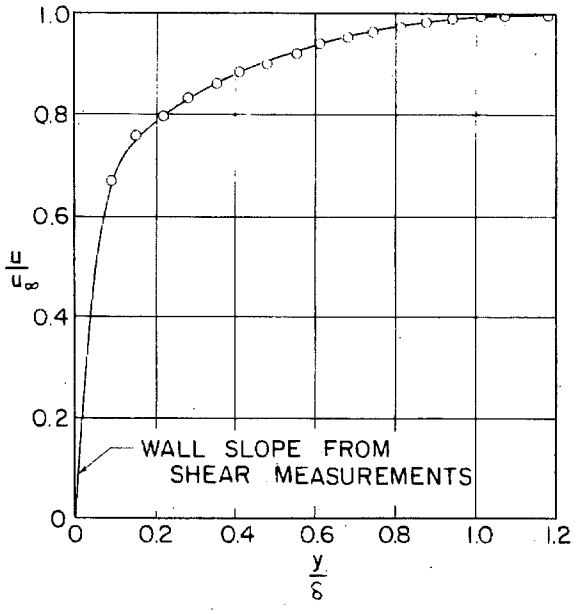

VELOCITY

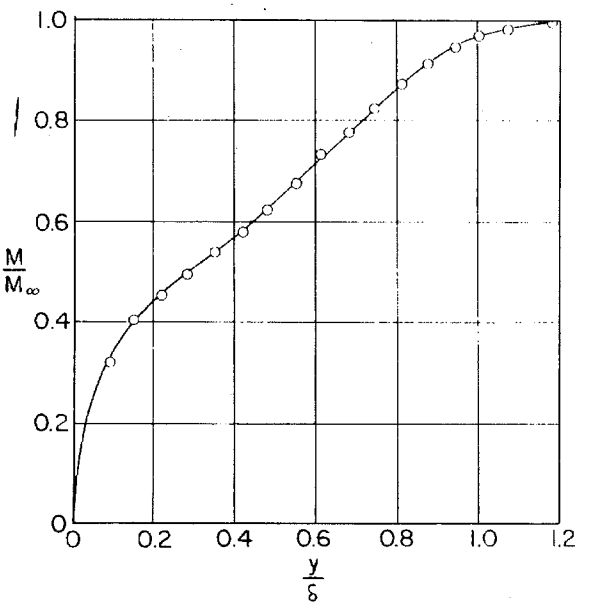

MACH NUMBER

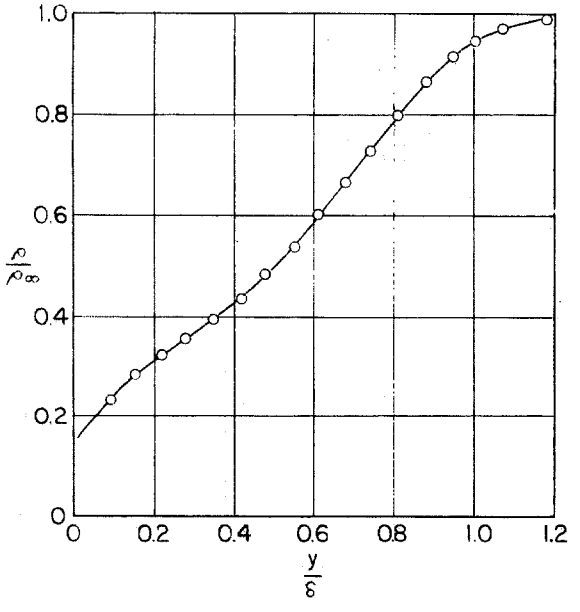

DENSITY

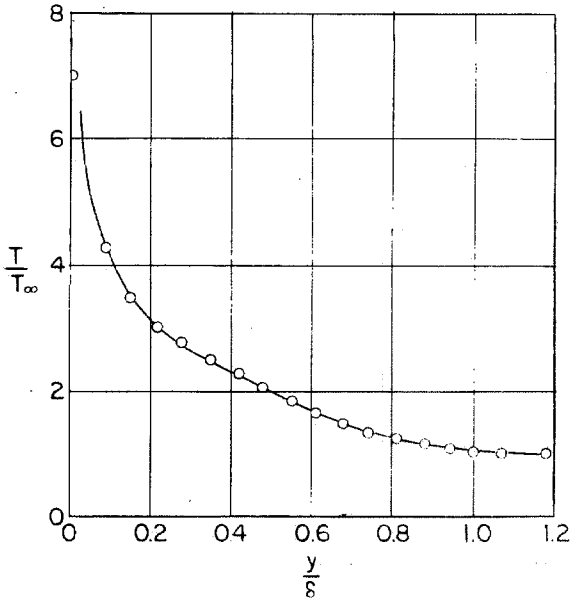

TEMPERATURE

δ = 0.457 in.
δ^* = 0.256 in.
θ = 0.0162 in.
R_θ = 4040
p_o = 109.4 psia, T_o = 225°F

DISTRIBUTION OF FLOW VARIABLES IN A TYPICAL TURBULENT BOUNDARY LAYER AT M = 5.8

FIG. 34

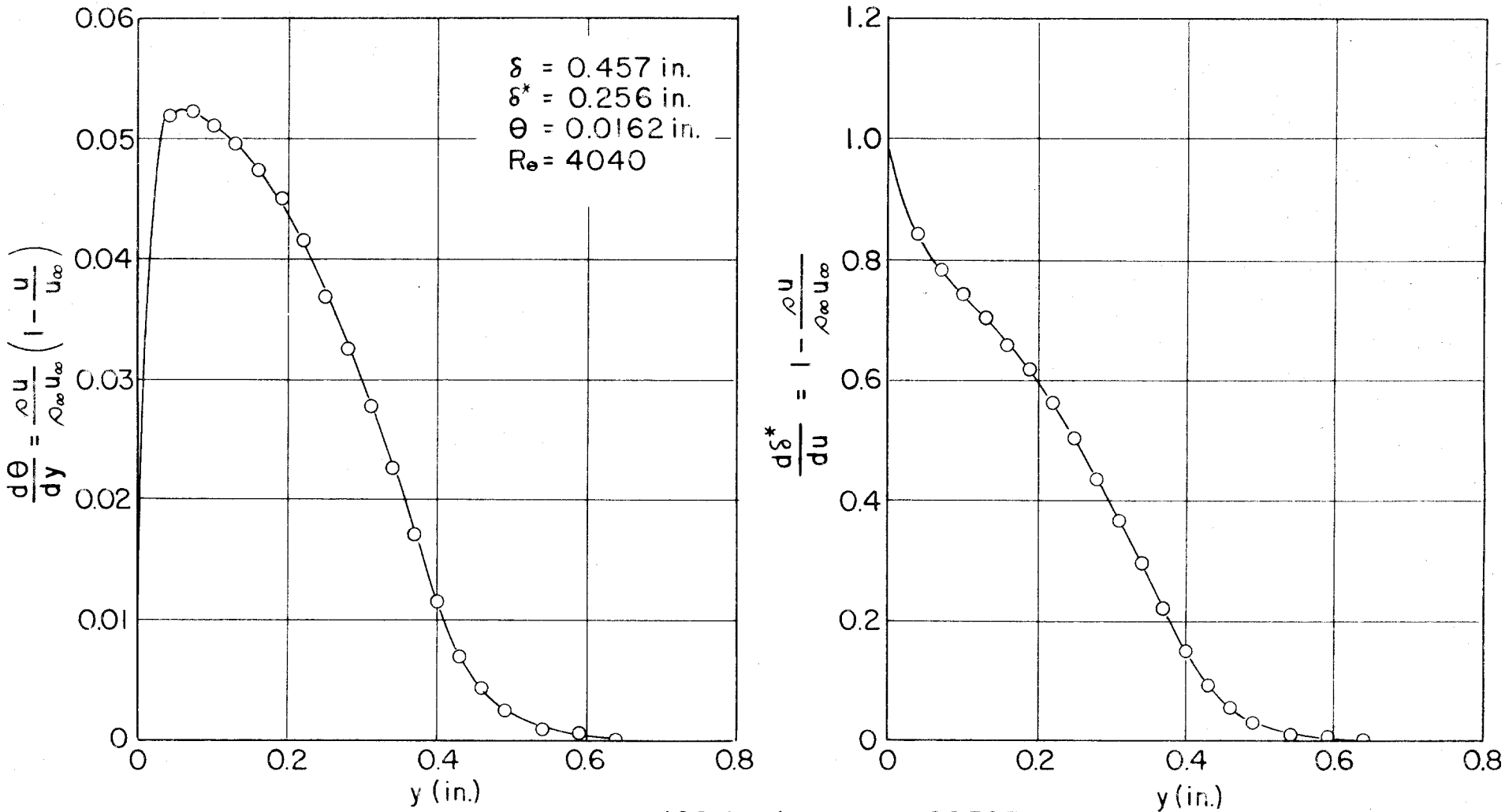

p_o = 109.4 psia, T_o = 225°F

TYPICAL MOMENTUM AND MASS DEFECT DISTRIBUTION IN A TURBULENT BOUNDARY LAYER AT M = 5.8

FIG. 35

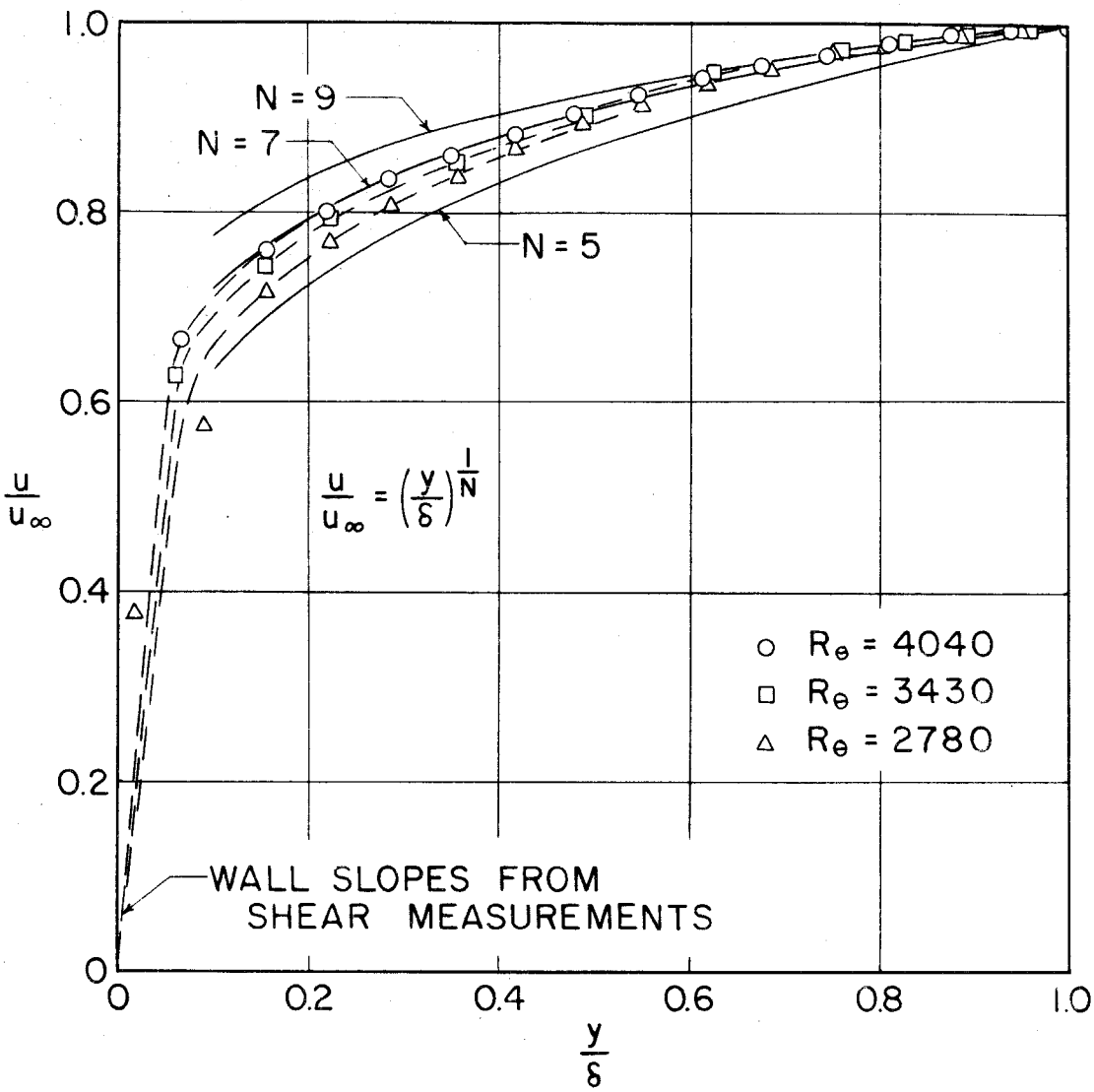

COMPARISON OF TURBULENT BOUNDARY LAYER VELOCITY PROFILES AT M = 5.8 WITH POWER LAW

FIG. 36

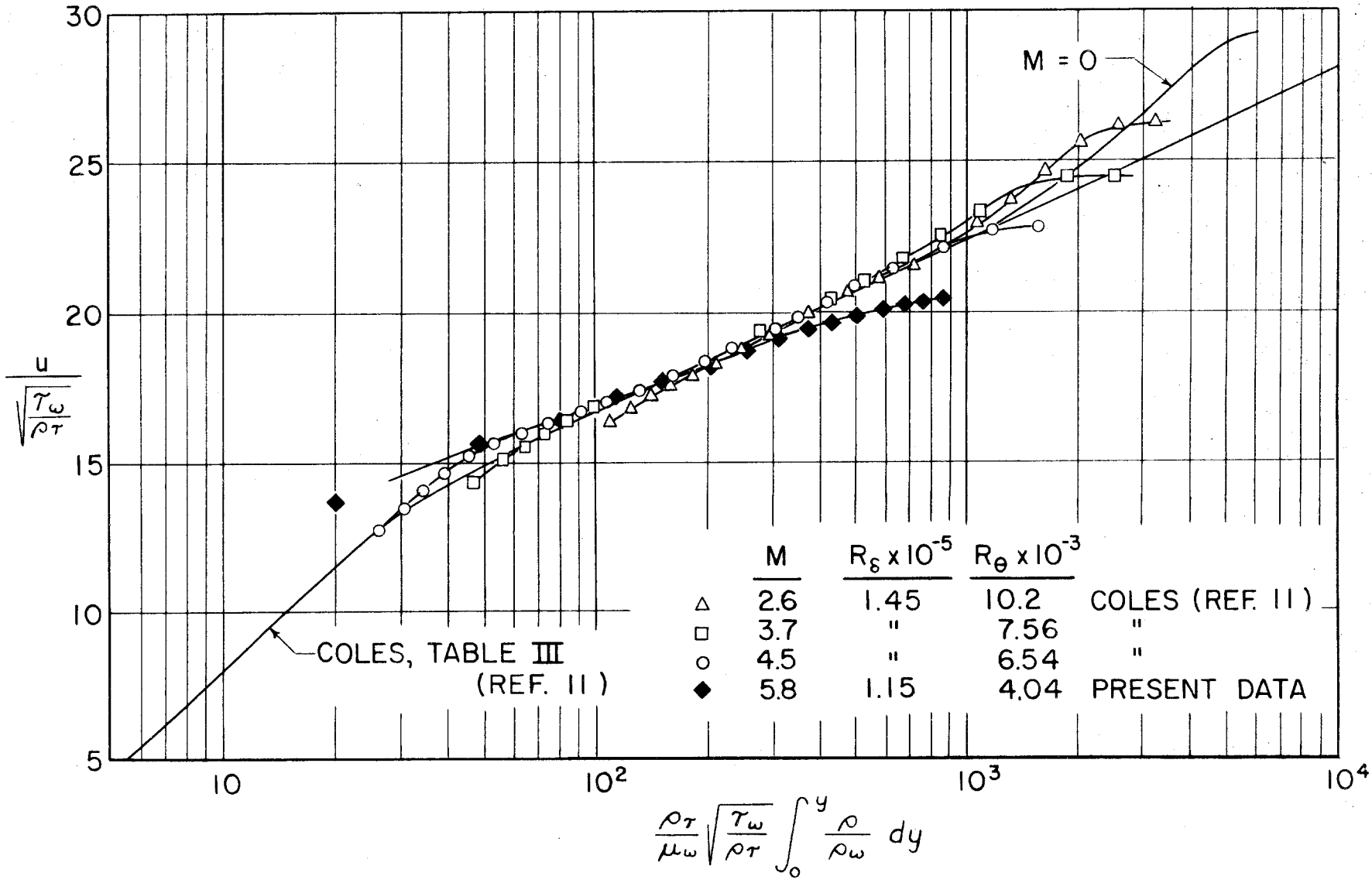

TURBULENT PROFILES ACCORDING TO FUNCTIONAL SIMILARITY

FIG. 37

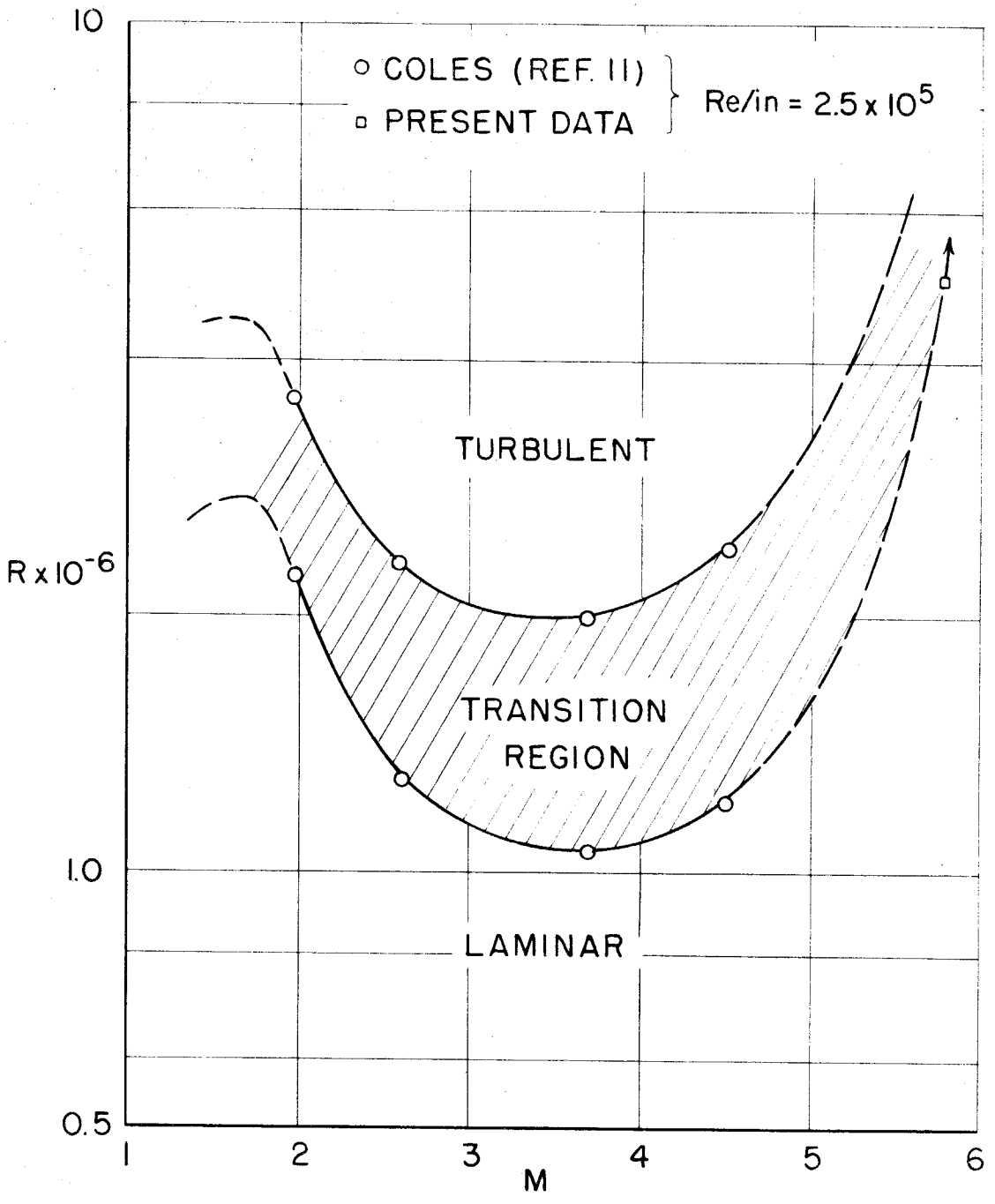

TRANSITION – MACH NUMBER TREND

FIG. 38

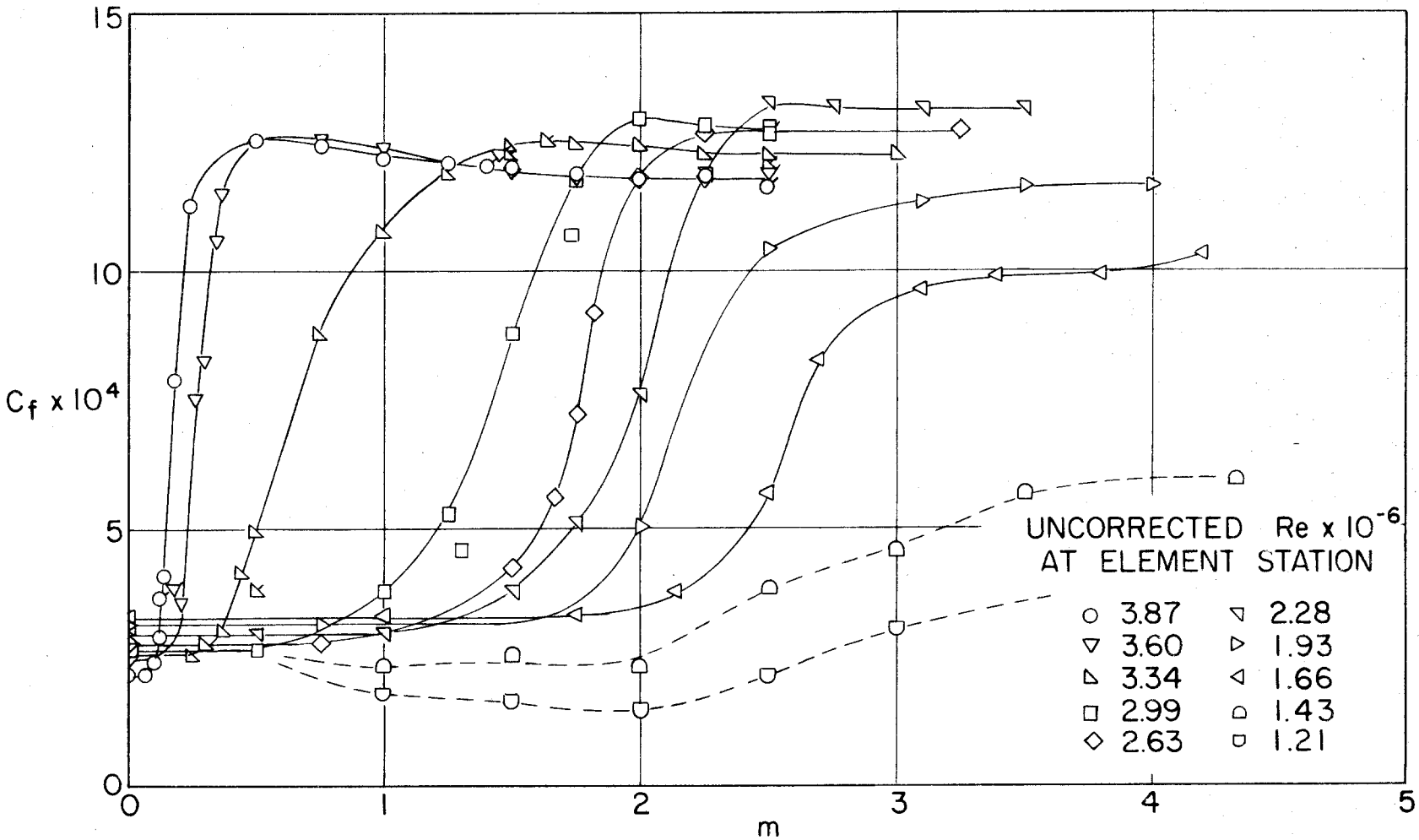

DEPENDENCE OF TRANSITION ON AIR MASS FLOW AT VARIOUS REYNOLDS NUMBERS

FIG. 39

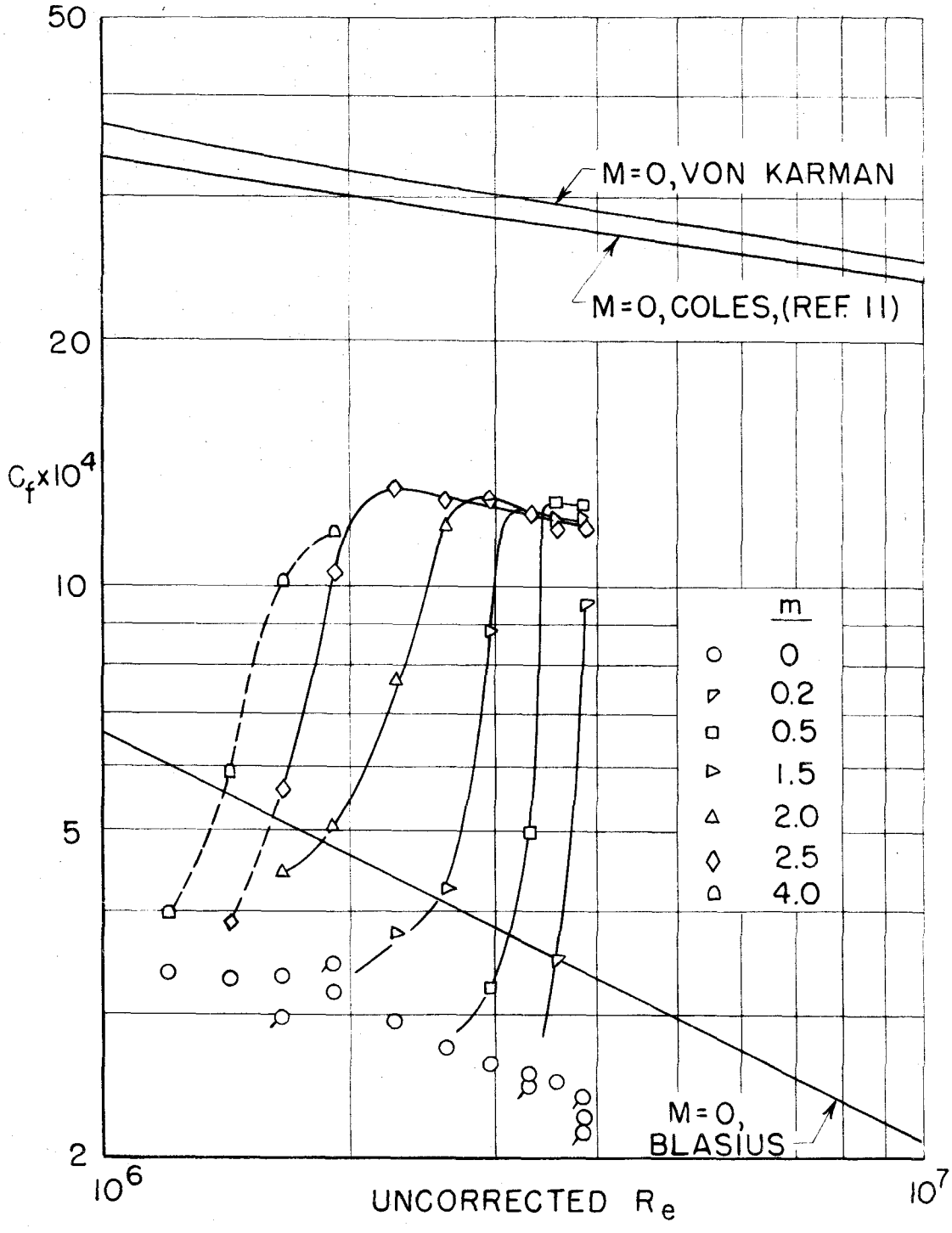

LOCAL SKIN FRICTION AT M=5.8

FIG. 40

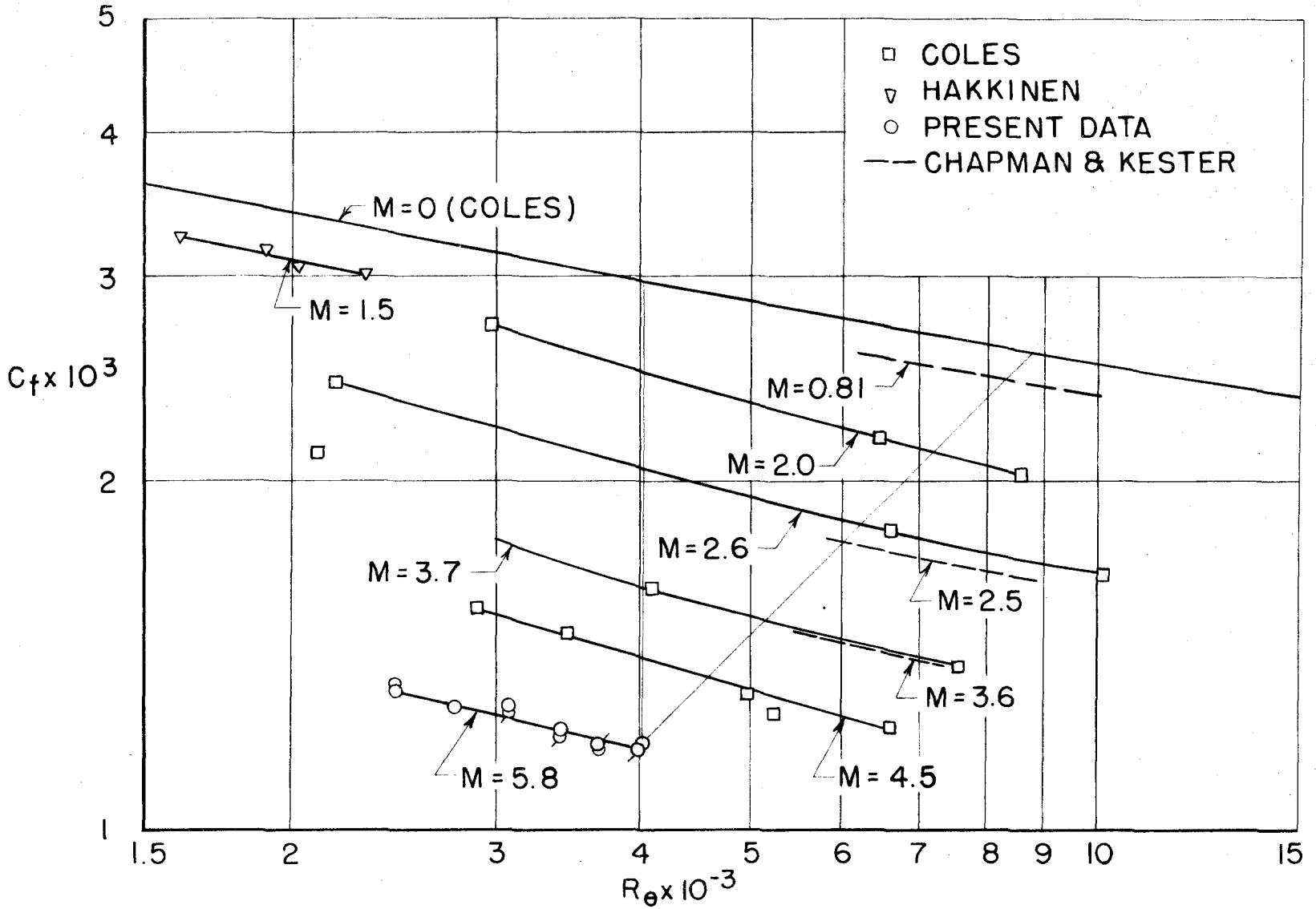

LOCAL TURBULENT SKIN FRICTION AS A FUNCTION OF R_θ

FIG. 41

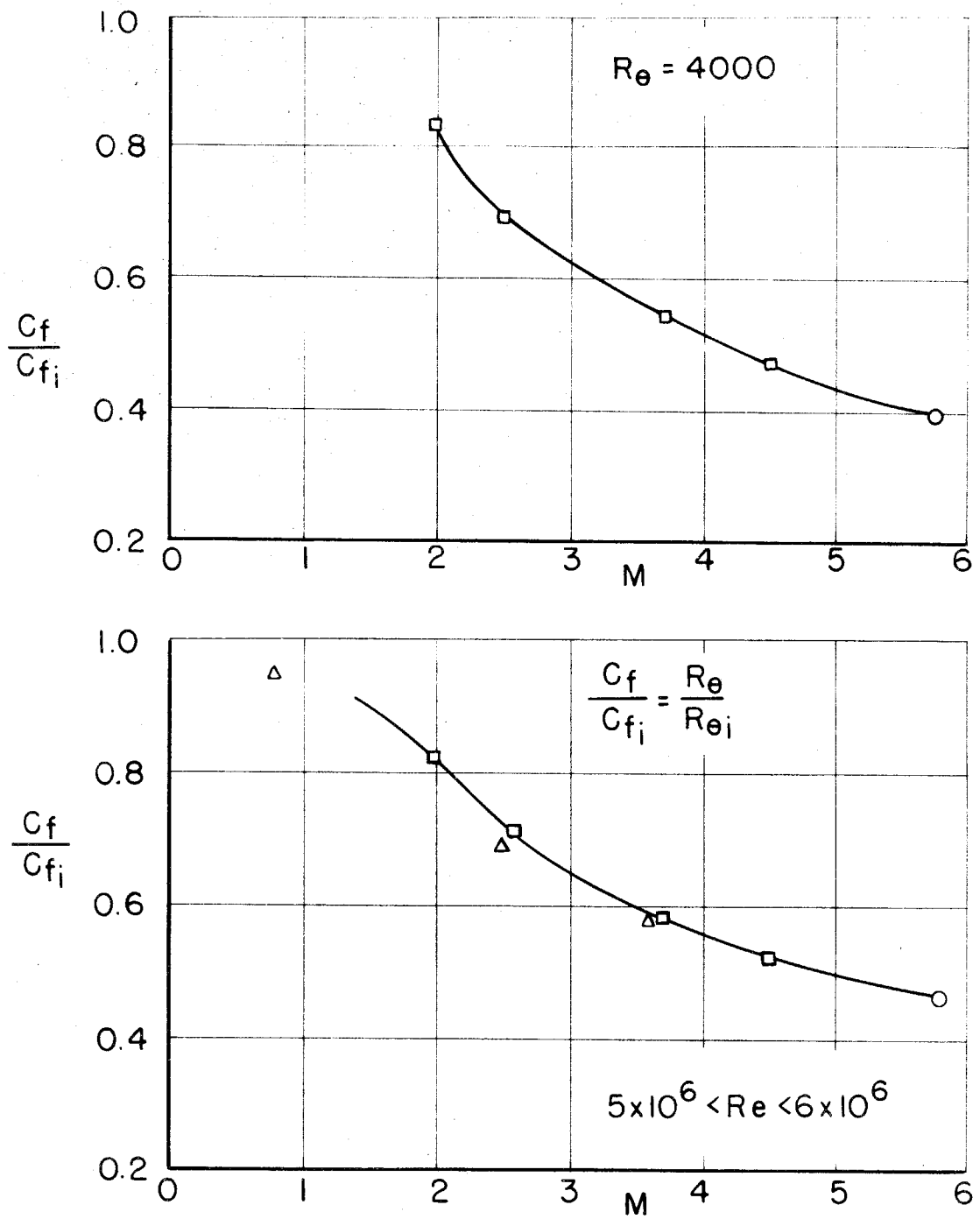

- ▫ COLES (FLAT PLATE)
- △ CHAPMAN & KESTER (CYLINDER, $L/D = 8$)
- ○ PRESENT DATA (FLAT PLATE)

C_{f_i} COLES (REF. 11, TABLE I)

VARIATION OF LOCAL TURBULENT SKIN FRICTION WITH MACH NUMBER

FIG. 42